

Ultrasound-Assisted Extraction of Total Saponins from *Aralia taibaiensis*: Process Optimization, Phytochemical Characterization, and Mechanism of α -Glucosidase Inhibition

Huan Li ^{1,2}
Bingtao Zhai^{1,2}
Jing Sun^{1,2}
Yu Fan³
Junbo Zou^{1,2}
Jiangxue Cheng^{1,2}
Xiaofei Zhang^{1,2}
Yajun Shi^{1,2}
Dongyan Guo^{1,2}

¹State Key Laboratory of Research & Development of Characteristic Qin Medicine Resources (Cultivation), Shaanxi University of Chinese Medicine, Xi'an, 712046, People's Republic of China; ²The Key Laboratory of Basic and New Drug Research of Traditional Chinese Medicine, Shaanxi University of Chinese Medicine, Xi'an, 712046, People's Republic of China; ³College of Basic Medicine, Shaanxi University of Chinese Medicine, Xi'an, 712046, People's Republic of China

Correspondence: Dongyan Guo
State Key Laboratory of Research & Development of Characteristic Qin Medicine Resources (Cultivation), Shaanxi University of Chinese Medicine, Xi'an, 712046, People's Republic of China
Tel +86 29-3818-5180
Email xmc2051080@163.com

Purpose: *Aralia taibaiensis*, a medicinal food plant, and total saponins from its root bark extract inhibit α -glucosidase activity, which is associated with type 2 diabetes; however, the inhibitory mechanism is unknown. Furthermore, a green extraction technique superior to conventional hot reflux extraction (HRE) is needed for the rapid and easy extraction of *A. taibaiensis* total saponins (TSAT) to exploit and utilize this resource. Our aim was to develop a green extraction method for obtaining TSAT and to investigate the mechanism by which TSAT inhibits α -glucosidase.

Materials and Methods: In this study, the ultrasound-assisted extraction (UAE) process was optimized using a Box–Behnken design, and the extraction mechanism was investigated using scanning electron microscopy (SEM). High-performance liquid chromatography (HPLC) was used for qualitative and quantitative analyses of TSAT. In vitro glycosylation assays, enzyme kinetics, fluorescence spectroscopy measurements, atomic force microscopy (AFM), Fourier transform infrared spectroscopy (FT-IR) and molecular docking techniques were used to investigate the mechanism by which the *A. taibaiensis* active ingredients inhibit α -glucosidase.

Results: The optimal parameters for the extraction yield were obtained as an ethanol concentration of 73%, ultrasound time of 34 min, ultrasound temperature of 61 °C and solid–liquid ratio of 16 g/mL, which were better than HRE. The SEM analysis showed that UAE effectively disrupted plant cells, thus increasing the TSAT yield. In vitro α -glucosidase inhibition experiments showed that both TSAT and its active ingredient, araloside A, inhibited α -glucosidase activity by binding to α -glucosidase, thereby changing the conformation and microenvironment of α -glucosidase to subsequently inhibit enzyme activity.

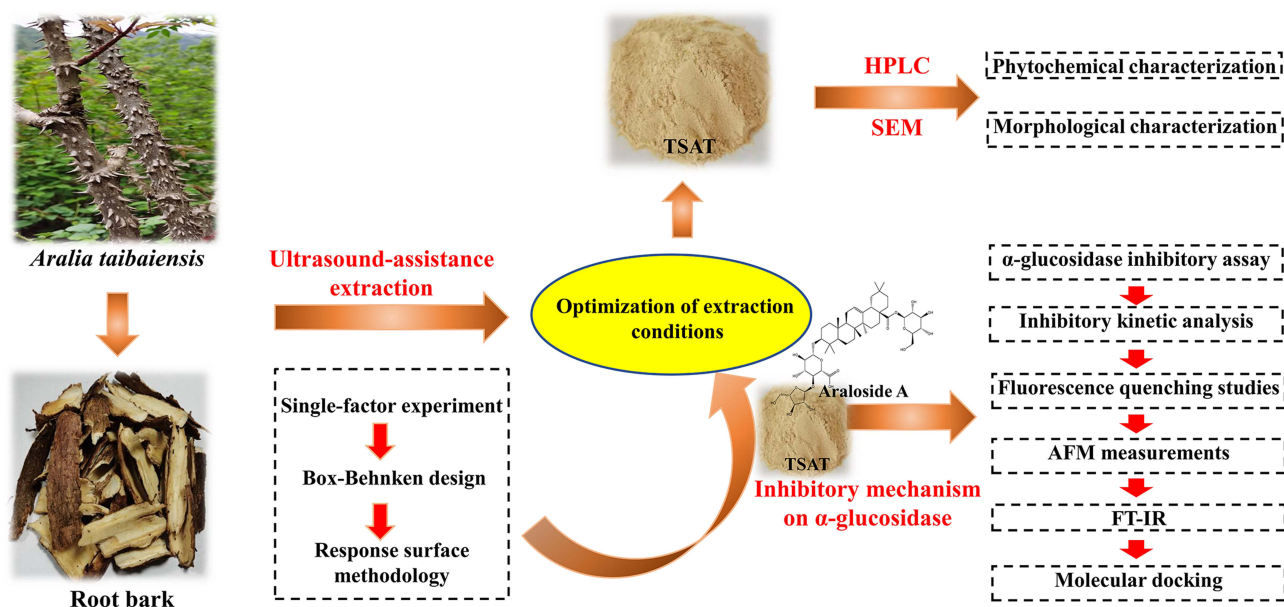
Conclusion: The optimal extraction conditions identified here established a basis for future scale-up of ultrasound extraction parameters with the potential for obtaining maximum yields. In vitro enzyme inhibition experiments investigated the mechanism of the TSAT interaction with α -glucosidase and further explored whether araloside A may be the main contributor to the good inhibition of α -glucosidase activity by TSAT.

Keywords: *Aralia taibaiensis* total saponins, ultrasound-assisted extraction, Box–Behnken design, α -glucosidase, inhibitory mechanism

Introduction

As one of the largest global health problems in the 21st century, diabetes is a metabolic disease characterized by elevated blood glucose levels that occurs when insulin production is inadequate or insulin is underutilized in the body.

Graphical Abstract



Postprandial hyperglycaemia is the main feature of type 2 diabetes and its complications. A common strategy to reduce blood sugar levels is to inhibit the activity of carbohydrate hydrolase, especially α -glucosidase located in the brush border of small intestinal epithelial cells.^{1,2} α -Glucosidase inhibitors improve postprandial hyperglycaemia by reducing enzyme activity and delaying the digestion of carbohydrates. Some drugs, such as acarbose, voglibose and miglitol, are common α -glucosidase inhibitors. However, in clinical applications, they often cause flatulence, abdominal pain and diarrhoea.³ Therefore, the identification of effective α -glucosidase inhibitors with few side effects is very important. Pentacyclic triterpene saponins are secondary metabolites that are widely distributed in various plants, including *Lagerstroemia*, *Schisandra* and *Xanthoceras sorbifolia Bunge*, and have been regarded as potential sources of therapeutic agents for diabetes due to their antihyperglycaemic properties.⁴⁻⁶ Hou et al⁷ reported that six pentacyclic triterpene compounds isolated from the leaves of *Lagerstroemia speciosa* exhibited good inhibitory activity against α -glucosidase. In addition, Ding et al reported that the pentacyclic triterpene saponin betulinic acid tightly binds to the active site of α -glucosidase, which might hinder the entrance of the substrate, leading to decreased enzyme activity.⁸

Aralia taibaiensis (Araliaceae) is a medicinal and edible plant that is widely distributed in the Qinba Mountains in western China.⁹ In China, *A. taibaiensis* root bark extract has been used to treat diabetes for many years, and its main active ingredients are pentacyclic triterpenoid saponins.¹⁰ Previous studies reported that the antidiabetic activity of *A. taibaiensis* is related to its high saponin content.¹¹ In addition, *A. taibaiensis* total saponins (TSAT) exert an inhibitory effect on α -glucosidase in vitro and possess antioxidant activity.^{11,12} Researchers have speculated that the C-3 position in the active ingredient structure, such as the β -D-glucopyranosyl-(1 \rightarrow 2)-[β -D-glucopyranosyl-(1 \rightarrow 3)]- β -D-glucuronopyranosyl oligosaccharide moiety, and other glycosyl substitutions are responsible for the antioxidant and antiglycosyl activities.¹³ However, to the best of our knowledge, these studies mainly focused on the inhibition of α -glucosidase activity but did not describe its inhibitory mechanism.

In addition, TSAT was obtained using traditional extraction methods, which were time-consuming, costly and inefficient. In recent years, ultrasound-assisted extraction (UAE) has recently attracted significant research interest due to its natural advantages over conventional methods, such as higher saponin content yields, faster release kinetics, shorter processing time, and greater economic value.¹⁴⁻¹⁶ When

ultrasound is applied, a strong mixing effect of the liquid medium is induced, producing cavitation bubbles. The explosion of the cavitation bubbles generates shock waves that lead to high shear and turbulence in the liquid medium and accelerate interparticle collisions. When cavitation bubbles explode continuously on or near the surface of the plant tissue matrix, the high velocity shock waves cause tissue surface flaking, erosion and particle fragmentation, which reduce the size of tissue particles, increase the surface area and disrupt the cellular junction structure of the plant matrix, thereby increasing mass transfer efficiency and improving extraction rates.^{17–20} However, the shortcomings of UAE are that the effective action area (ultrasonic) is restricted by the ultrasonic attenuation factor. If the diameter of the extraction tank is too large, an ultrasonic blank area is formed on the peripheral wall of the tank.²¹ Admittedly, the extraction rate of active plant components is usually influenced by factors such as temperature, time, liquid to solid ratio, ultrasound power and solvent polarity.^{22–24} Therefore, the extraction process must be optimized to maximize the extraction rate and pharmacological effects of bioactive substances. The response surface method (RSM) is a widely used mathematical and statistical tool for optimizing extraction processes to account for the interaction of independent variables.²⁵ The Box–Behnken design (BBD), one type of RSM, is easier to interpret and perform than other designs.²⁶

To the best of our knowledge, no studies have reported the optimization of TSAT with UAE based on yield, and the lack of understanding of the *in vitro* hypoglycaemic mechanism of TSAT and its active compounds has limited the development and utilization of *A. taibaiensis*. This study aimed to use BBD-RSM to determine the best condition for UAE of TSAT and obtain the best yield. In addition, using enzyme kinetic analyses, fluorescence quenching, AFM, FT-IR and molecular docking, the mechanism of action of TSAT and its active compounds on α -glucosidase was thoroughly studied. This research will provide new insights into the development and utilization of *A. taibaiensis* to consolidate its many valuable pharmacological attributes.

Materials and Methods

Materials and Chemicals

Tarasaponin IV ($\geq 98\%$, Lot number: HS191222B1), araloside C ($\geq 98\%$, Lot number: HS191219B1), stipuleanoside R2 ($\geq 98\%$, Lot number: HS191221B1), pseudoginsenoside

RT1 ($\geq 98\%$, Lot number: HS191224B1), araloside A ($\geq 98\%$, Lot number: 18091305) and Chikusetsu saponin Iva ($\geq 98\%$, Lot number: 111861–201001) standards were provided by Chenguang Biotechnology Co., Ltd. (Baoji, China). Ascorbic acid were obtained from Sigma–Aldrich (St. Louis, MO, USA). Acarbose α -glucosidase (EC 3.2.1.20) from *Saccharomyces cerevisiae* was obtained from Shanghai Yuan Ye Biotechnology Co., Ltd. (Shanghai, China) and was dissolved in sodium phosphate buffer (0.1 M, pH 6.8). Acarbose and p-nitrophenyl- α -D-glucopyranoside (pNPG), which were purchased from Sigma–Aldrich Co. (St Louis, MO, USA), were both dissolved in sodium phosphate buffer. The DMSO content was less than 0.2% and had no effect on the activity of α -glucosidase in the present study. HPLC-grade acetonitrile was obtained from Thermo Fisher Scientific Co. (Waltham, MA, USA). All other reagents used were of analytical grade and purchased from Aladdin (Shanghai, China), and ultra-pure water was used throughout the whole experiment.

Plant Material

The root bark of *A. taibaiensis* was collected in the Qinba Mountains, Shaanxi Province, China, and was botanically identified by Dr. Jitao Wang (Shaanxi University of Chinese Medicine). A voucher specimen (SUCM, No. 20201003) was deposited in the Herbarium of Shaanxi University of Chinese Medicine. *A. taibaiensis* root bark was washed with double distilled water, dried at 60 °C and crushed. Before the experiment, the powder was placed in a cool and dry place.

UAE Procedure

The UAE of TSAT was performed in a water-bath sonicator (KQ500DE, Ultrasonic Instrument Factory, Kunshan city, China). The effects of different variables, such as the solvent concentration, ultrasound power, ultrasound time, ultrasound temperature, liquid to solid ratio and number of extractions, are known to affect the extraction rate. In this case, six process variables, ie, the ethanol concentration (%), ultrasound power (W), ultrasound time (min), ultrasound temperature (°C), solid–liquid ratio (g/mL) and number of extractions, were tested in a preliminary experiment to determine the effects of factors and levels on the TSAT extraction process (shown in Table 1). All operations were performed three times in parallel, and the optimum extraction process was determined based on the maximum yield of TSAT.

Table 1 Design of the Single Factor Experiment

Independent Variable	Factor Level
Ethanol concentration (%)	50, 60, 70, 80, 90
Ultrasound time (min)	10, 20, 30, 40, 50
Ultrasound temperature (°C)	40, 50, 60, 70, 80
Solid-liquid ratio (g/mL)	5, 10, 15, 20, 25
Ultrasound power (W)	100, 200, 300, 400, 500
Numbers of extraction	1, 2, 3, 4, 5

Optimization by RSM

BBD-RSM was used to optimize the extraction process parameters and to obtain their interactions based on the results of single-factor tests. The effects of independent variables of UAE on the TSAT contents were investigated using the following indicators: ethanol concentration (%) (X_1), ultrasound time (min) (X_2), ultrasound temperature (°C) (X_3) and solid-liquid ratio (g/mL) (X_4). A mathematical second-order polynomial regression equation was used to calculate the value of Y, as shown in Equation (1):

$$Y = \beta_0 + \sum_{j=1}^4 \beta_j X_j + \sum_{j=1}^4 \beta_{jj} X_j^2 + \sum_{i=1}^3 \sum_{j=i+1}^4 \beta_{ij} X_i X_j \quad (1)$$

where Y is the response variable; β_0 is a fixed value that indicates the intercept of the model; β_j , β_{jj} and β_{ij} are the linear, quadratic and interactive coefficients, respectively; and X_i and X_j represent the coded level of independent variables.

Conventional Heat Reflux Extraction (HRE)

A comparison between the HRE and UAE was carried out to estimate the efficiency of the UAE process established in the present study. The HRE of TSAT from was performed under the optimized UAE conditions with slight modifications. Briefly, 5.0 g of the preprepared sample were extracted three times under reflux with 75 mL of 70% ethanol at 78°C, each time for 2 h. After HRE, the combined extract solution was then concentrated in vacuo, and the extract was stored at 4°C until further analysis.

Determination of TSAT

The total saponin content of the extracts was determined using the method described by Hu et al with slight

modifications.²³ The TSAT content was reported as equivalents of oleanolic acid, and the absorbance was recorded immediately at 545 nm using a UV-Vis spectrophotometer (UV-2600, Shimadzu, Kyoto, Japan). The regression equation of the oleanolic acid standard curve was obtained as $Y = 38.062X - 0.2648$ ($R^2 = 0.9993$).

Regarding the method for standard curve preparation, 1 mL of prepared sample was used for standard curve preparation, and 1 mL of prepared sample was added to measure the saponin content in the extract. The total saponins extraction rate was calculated. The yield rate of TSAT was calculated using the following equation:

$$\text{Yield\%} = \frac{C \times V}{m} \times 100\% \quad (2)$$

where C is the saponin content in prepared samples (mg/mL), V is the volume of prepared samples (mL), and m is the weight of prepared samples (mg).

HPLC Analysis

The conditions for the HPLC analysis were based on previous studies with slight modifications.²⁷ The purified TSAT was analysed using an HPLC-DAD system (Agilent 1260 series liquid chromatograph, USA) equipped with a COSMOSIL5C18-MS-II chromatography column (5 μ m, 250 mm \times 4.6 mm id). The mobile phase consisted of acetonitrile (solvent A) and a 0.1% aqueous phosphoric acid solution (V/V) (solvent B). The elution procedure was as follows: 0–10 min, 5–20% A; 10–25 min 20–28% A; 25–35 min, 28–33% A; 35–45 min, 33–38% A; 45–55 min, 38–46% A; 55–60 min, 46–60% A; 60–68 min, 60–75% A; and 68–70 min, 75–45% A. The operating conditions of the instrument were a temperature of 30°C and a flow rate of 0.8 mL/min. The injection volumes of standards and samples were 10 μ L. The detection wavelength was set to 203 nm. Before injection, all samples were passed through a 0.22 μ m filter. After matching with the standard, the peak was determined based on the retention time. The linear calibration curve of the standard was used for quantification.

Method Validation

The method was validated for linearity, limit of detection (LOD), limit of quantification (LOQ), precision (interday and intraday precision), stability, accuracy and recovery rate according to the International Conference on Harmonization (ICH) guidelines and previous reports.^{28,29}

Morphology

The surface structure of treated samples was analysed and compared with untreated *A. taibaiensis* powder using VEGA3-TESCAN.

α -Glucosidase Inhibition Assay

An α -glucosidase inhibition assay was performed as previously described with minor modifications.³ The reaction system consisted of 50 μ L of 0.2 M potassium phosphate buffer (pH 6.8), 50 μ L of test sample (25–500 μ g/mL) and 100 μ L of 0.1 U/mL α -glucosidase. It was incubated at 37°C for 10 min. Then, 50 μ L of a 5 mM pNPG solution were added. The enzymatic reaction was incubated at 37°C for 10 min. The reaction was finally terminated by adding 50 μ L of 1 mol/L Na₂CO₃. The absorbance of p-nitrophenol was measured at 405 nm using a microplate reader. Acarbose was used as a positive control. The experiments were conducted three times in parallel. α -Glucosidase inhibition was calculated using the following equation:

$$\text{Inhibition(\%)} = \frac{A_0 - (A_1 - A_2)}{A_0} \times 100 \quad (3)$$

where A_0 represents the absorbance of the negative control without the sample; A_1 represents the test system containing the sample; A_2 represents the absorbance of the blank system. The IC₅₀ value was calculated.

Inhibitory Kinetic Analysis

The kinetic models of TSAT and araloside A versus α -glucosidase were determined by performing an enzyme activity assay. The reaction rate was determined by changing the concentrations of the substrate and inhibitor. The inhibition type and mechanism were analysed by constructing Lineweaver–Burk plots of the enzyme reaction velocity (v) versus the substrate concentration, and the relevant parameters were calculated using the following equations:

$$\frac{1}{V} = \frac{K_m}{V_{\max}} \left(1 + \frac{[I]}{K_i} \right) \frac{1}{[S]} + \frac{1}{V_{\max}} \quad (4)$$

The secondary plots were constructed from:

$$\text{Slope} = \frac{K_m}{V_{\max}} + \frac{K_m[I]}{V_{\max}K_i} \quad (5)$$

where V is the enzyme reaction rate, V_{\max} is the maximum enzyme reaction rate, $[S]$ denotes the concentration of substrate, $[I]$ represents the concentrations of TSAT and

araloside A, and k_m represents the Michaelis–Menten constant.

Fluorescence Quenching Studies

Fluorescence quenching studies were performed using a spectrofluorometer (model F-7000 Hitachi, Tokyo, Japan) as described in the study by Wei-Ming et al,³⁰ with some modifications. Fluorescence spectra were measured at two different temperatures (298 K and 310 K) in the range of 298–370 nm with an excitation wavelength of 280 nm. The excitation and emission bandwidths were both set to 2 nm. Different concentrations of TSAT and araloside A were added to the buffer solution (0.1 M sodium phosphate buffer, pH 6.9) containing a fixed amount of α -glucosidase (0.1 U/mL). All the mixtures were incubated for 10 min to equilibrate before measurements were recorded. The fluorescence spectra of the buffer were subtracted as the background fluorescence.

AFM Measurements

Twenty microliters of α -glucosidase (0.1 U/mL) with or without 20 μ L of araloside A (0.02 mg/mL) were incubated at 37°C for 1 h, added to the mica substrate and dried at room temperature for 12 h. AFM measurements were determined in air using a Bruker MM8 instrument (USA).

FT-IR Spectroscopy

The FT-IR spectra of α -glucosidase (0.1 U/mL) and its araloside A- α -glucosidase complex were measured in the range of 4000–500 cm⁻¹ in sodium phosphate buffer, pH 7.0, at room temperature. All spectra were recorded using the ATR method with a resolution of 4 cm⁻¹ and 60 scans. The final concentration of araloside A was 0.2 mg/mL. The corresponding absorbance values of free araloside A and buffer solutions were recorded with the same instrumental parameters and subtracted. The curves were fitted using Origin software (version 8.0, Origin Lab, Northampton, MA, USA).

Molecular Docking

Molecular docking was applied to determine the possible binding site(s) between acarbose, araloside A and α -glucosidase. The structure of α -glucosidase was determined through homology modelling (PDB ID: 3A4A). After removing extraneous small molecules from protein molecules using PyMOL 2.3 software, protein molecules were imported into AutoDock Tools-1.5.6 software to remove

water molecules, hydrogen atoms were added, and the structures were saved as pdbqt files. Small-molecule compounds were imported into AutoDock Tools-1.5.6 software, water molecules were removed, atomic charges were added, atom types were assigned, all flexible bonds were made rotatable by default, and the files were saved as pdbqt files. All docking experiments were performed using AutoDock Tools-1.5.6 software. During the calculations, an 80x80x70 dot matrix module with 0.375 intervals and centre settings (-15.640, -35.005, -3.958) was used. Molecular docking calculations were performed using the Lamarckian genetic algorithm with the following parameters: a population of 150, a maximum of 25 million energy evaluations, a maximum number of 2000, a crossover rate of 0.8, a mutation rate of 0.02, 50 independent docking runs and an evaluation of the final docking structure based on the binding free energy. Docking results were visualized using PyMOL 2.3 software.

Statistical Analysis

Design-Expert version 10 software (Stat-Ease Inc., Minneapolis, MN, USA) was employed for the RSM design and statistical analysis. Differences between the means were considered statistically significant at $p < 0.05$. All experiments were repeated in triplicate, and the values are presented as the means \pm standard deviations (S.D.). The experimental analyses and calculations were performed using GraphPad Prism 6 software (La Jolla, CA, USA).

Results and Discussion

Single-Factor Experiments

Figure 1 shows the effect of each factor on the total saponin contents. Figure 1A shows the trend of increasing TSAT yields with an increasing number of extractions. The yield decreased slightly when more than 3 extractions were performed, and the process consumed excess energy and time. Thus, 3 extractions are considered optimal. Ultrasound power significantly affects the yield. As shown in Figure 1B, the yield increased with increasing ultrasound power due to the increased amplitude of the ultrasound waves passing through the solvent, resulting in increased “acoustic cavitation”. However, above 400 W, the drift of the extraction was accelerated, and consequently, the efficiency of the ultrasonic energy transfer into the medium was reduced, resulting in lower yields.^{31,32} As the ethanol concentration increases from

50% to 70%, the total saponin yield increased steadily, reaching a peak at 70% (Figure 1C). According to the theory of similarity and phase solubility, the release of components from the cells is facilitated when the polarities of the solute and solvent are similar.^{15,33} Extraction time affects the surface contact between the solute and solvent. As shown in Figure 1D, increasing the ultrasound time from 10 min to 30 min resulted in a significant increase in yield, which was attributed to the prolonged contact time between the solute and solvent that facilitated the diffusion of the target compound. However, prolonged extraction was not suitable for the extraction of bioactive compounds, probably due to the degradation of the components.³⁴ In the present study, the ultrasound time was chosen to be 30 min. As shown in Figure 1E, a regular increase in yield was observed when the temperature increased to 60°C. The maximum yield was obtained at 60°C, the temperature that increased the solubility of the saponins and accelerated the molecular movement of the solute.³⁵ As shown in Figure 1F, the greater the amount of solvent, the greater the contact area, and the stronger the ultrasound waves applied to the plant surface, leading to greater fragmentation, erosion and pore formation effects and resulting in higher yields. However, as the solid–liquid ratio increased, saponin yields tended to decrease. This result may be attributed to the enhanced cavitation effect, resulting in the production of more impurities that hinder the dissolution of the saponins.^{23,32} In the present study, the maximum yield was obtained at a solid–liquid ratio of 15 g/mL.

Optimization of TSAT Extraction by BBD Model Fitting and Statistical Analysis

Based on the results of previous single-factor experiments, the ethanol concentration (%), ultrasound time (min), ultrasound temperature (°C) and solid–liquid ratio (g/mL) were selected as the main influencing factors. The experimental design matrix of the independent variables used for the RSM and their codes and levels are shown in Table 2. The results of 29 experimental runs using the Box–Behnken design along with the measured and predicted values for both responses for each trial in the experimental design are shown in Table 3.

The ANOVA results are presented in Table 4. The p value was calculated to evaluate the significance of each coefficient and indicate the interaction pattern between the variables. X_1 , X_2 , X_4 , X_1X_2 , X_1X_4 and

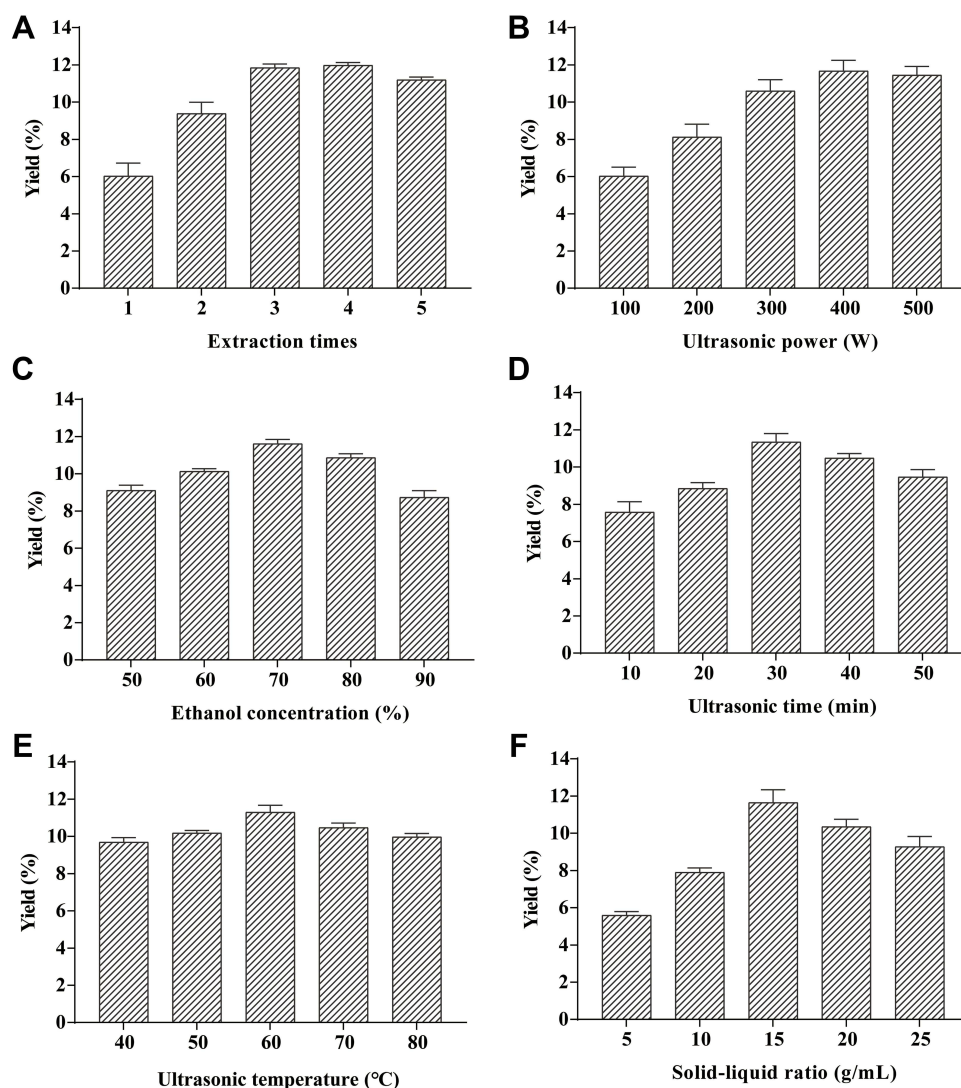


Figure 1 Effect of different factors on the extraction yield of TSAT. (A) extraction times, (B) ultrasonic power, (C) ethanol concentration, (D) ultrasound time, (E) ultrasound temperature and (F) solid-liquid ratio.

X_2X_4 were significant ($p < 0.05$), while X_3 , X_1X_3 and X_2X_3 were not ($p > 0.05$). One-way ANOVA indicated that the model was highly significant ($p < 0.0001$) with high F values (15.64). The correlation coefficient (R^2) for Y is

Table 2 Variables and Their Levels Used in the Experiments

Independent Variables	Levels		
	-I	0	I
Ethanol concentration (%)	60	70	80
Ultrasound time (min)	20	30	40
Ultrasound temperature (°C)	50	60	70
Solid-liquid ratio	10	15	20

0.9399, and the R^2 value was calculated to judge the adequacy of the model. The results indicate that the model developed here was significant ($p < 0.0001$). The R^2_{pred} of 0.6997 is reasonably consistent with the R^2_{adj} of 0.8798, and the difference is less than 0.2. The value of R^2_{adj} indicated a total variation of 88% in the total saponin yield attributable to the independent variables. Additionally, the low value of the CV (2.03%) implies high precision and good reliability of the actual values. Adeq precision (AP) (value is 13.87) compares the range of the predicted values at the design points to the average prediction error. Ratios greater than 4 indicate adequate model discrimination. The model can be used to navigate the design space.

Table 3 Experimental Design and Observed Response

Run	Ethanol Concentration (%)	Ultrasonic Time (min)	Ultrasonic Temperature (°C)	Solid-Liquid Ratio (g/mL)	Yield (%)	
					Actual	Predicted
1	0 (70)	-1 (20)	-1 (50)	0 (15)	10.39	10.41
2	0 (70)	-1 (20)	0 (60)	-1 (10)	10.79	10.70
3	0 (70)	-1 (20)	1 (70)	0 (15)	11.06	10.94
4	0 (70)	0 ((30)	0 (60)	0 (15)	11.57	11.72
5	0 (70)	-1 (20)	0 (60)	1 (20)	10.56	10.39
6	1 (80)	0 (30)	0 (60)	1 (20)	10.95	10.97
7	0 (70)	0 (30)	-1 (50)	1 (20)	11.02	10.97
8	-1 (60)	0 (30)	1 (70)	0 (15)	9.91	10.17
9	0 (70)	0 (30)	0 (60)	0 (15)	11.62	11.72
10	0 (70)	0 (30)	1 (70)	-1 (10)	10.83	10.88
11	-1 (60)	0 (30)	0 (60)	-1 (10)	9.73	9.56
12	0 (70)	1 (40)	1 (70)	0 (15)	11.46	11.29
13	-1 (60)	1 (40)	0 (60)	0 (15)	10.91	10.63
14	1 (80)	0 (30)	0 (60)	-1 (10)	11.23	11.13
15	0 (70)	1 (40)	-1 (50)	0 (15)	11.34	11.31
16	1 (80)	0 (30)	1 (70)	0 (15)	11.41	11.37
17	1 (80)	-1 (20)	0 (60)	0 (15)	10.77	11.06
18	0 (70)	0 (30)	0 (60)	0 (15)	11.73	11.72
19	1 (80)	1 (40)	0 (60)	0 (15)	11.25	11.20
20	0 (70)	0 (30)	1 (70)	1 (20)	11.18	11.19
21	0 (70)	1 (40)	0 (60)	1 (20)	11.45	11.68
22	0 (70)	0 (30)	0 (60)	0 (15)	12.02	11.72
23	0 (70)	1 (40)	0 (60)	-1 (10)	10.36	10.67
24	0 (70)	0 (30)	0 (60)	0 (15)	11.67	11.72
25	-1 (60)	0 (30)	-1 (50)	0 (15)	9.87	10.05
26	-1 (60)	0 (30)	0 (60)	1 (20)	10.46	10.41
27	0 (70)	0 (30)	-1 (50)	-1 (10)	10.58	10.58
28	-1 (60)	-1 (20)	0 (60)	0 (15)	9.45	9.51
29	1 (80)	0 (30)	-1 (50)	0 (15)	11.09	10.97

Table 4 ANOVA for Regress Equation

Source	Sum of Squares	df	Mean Square	F-value	p-value	Significant
Model	10.77	14	0.7694	15.64	<0.0001	Significant
X ₁	3.38	1	3.38	68.75	<0.0001	**
X ₂	1.17	1	1.17	23.83	0.0002	**
X ₃	0.2028	1	0.2028	4.12	0.0617	
X ₄	0.3675	1	0.3675	7.47	0.0162	*
X ₁ X ₂	0.2401	1	0.2401	4.88	0.0443	*
X ₁ X ₃	0.0196	1	0.0196	0.3985	0.5380	
X ₁ X ₄	0.2550	1	0.2550	5.18	0.0390	*
X ₂ X ₃	0.0756	1	0.0756	1.54	0.2354	
X ₂ X ₄	0.4356	1	0.4356	8.86	0.0100	*
X ₃ X ₄	0.0020	1	0.0020	0.0412	0.8421	
X ₁ ²	3.50	1	3.50	71.11	<0.0001	**
X ₂ ²	0.9832	1	0.9832	19.99	0.0005	**
X ₃ ²	0.7747	1	0.7747	15.75	0.0014	**
X ₄ ²	1.44	1	1.44	29.20	<0.0001	**
Residual	0.6886	14	0.0492			
Lack of Fit	0.5635	10	0.0564	1.80	0.2996	Not significant
Pure Error	0.1251	4	0.0313			
Cor Total	11.46	28				
C.V.%	2.03					
		R ² = 0.9399	R ² adj = 0.8798	R ² pred = 0.6997		

Notes: *P<0.05, **P<0.01.

The following second-order polynomial equation was generated to analyse the effects of independent variables on the total saponin extraction yield:

$$\text{Yield (\%)} = 11.72 + 0.5308X_1 + 0.3125X_2 + 0.1300X_3 + 0.1750X_4 - 0.2450X_1X_2 + 0.0700X_1X_3 - 0.2525X_1X_4 - 0.1375X_2X_3 + 0.3300X_2X_4 - 0.0225X_3X_4 - 0.7343X_1^2 - 0.3893X_2^2 - 0.3456X_3^2 - 0.4706X_4^2$$

The fitted model must often be checked to ensure that it adequately approximates the actual system. The residuals of the least square method are critical for determining the adequacy of a model. As shown in Figure 2A, the predicted values were very close to the experimental values. Internal studentised residuals were analysed by constructing satisfactory model fits for the experimental runs, which showed that all data points were within the limits (Figure 2B). Figure 2C

shows the normal probability of the response residual plot and is normally distributed, as the points are reasonably close to the straight line and no variance bias is observed. The model effectively enhances the relationship between the process variables and the responses. Box-Cox plots of the power transformations of the variables (Figure 2D) show the perturbations of the variables within the determined range. These plots are satisfactory; therefore, we concluded that the empirical model is adequate for describing the total saponin extraction yield in the response surface plot.

Analysis of the Response Surface and Contour Plots

Response surface plots were generated by Design-Expert software to explain the interactions between the variables

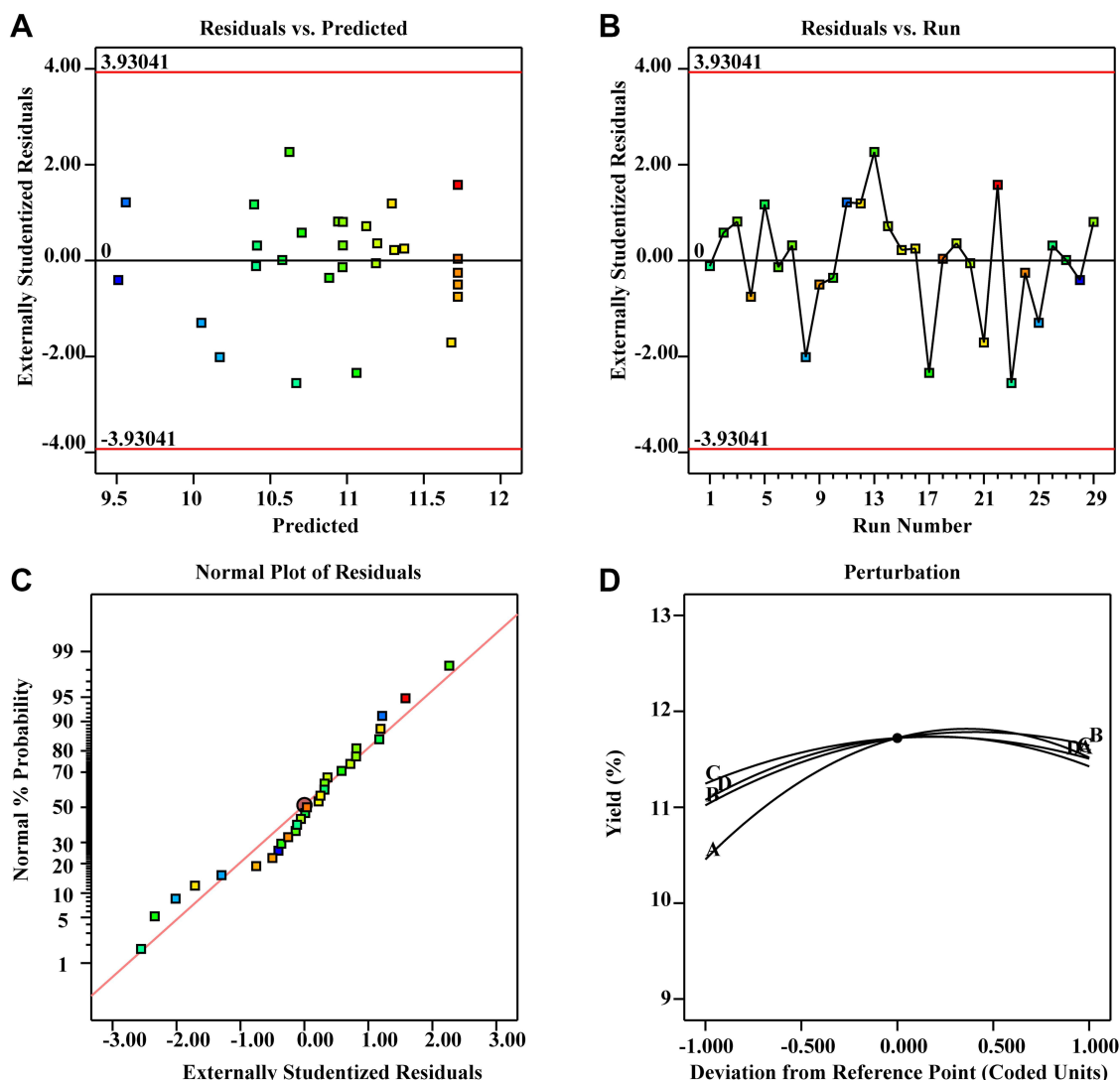


Figure 2 Diagnostic plots for the Box–Behnken model adequacy of the tested variable (predicted vs actual) against the TSAT yield. (A) Residuals vs predicted; (B) residuals vs run; (C) normal plot of residuals; (D) perturbation.

and to determine the optimum level of each variable that would obtain the maximum response value. The 3D response surface plots are shown in Figure 3. Surface ellipses typically indicate interaction effects between two independent variables on the dependent variable, with circles indicating opposite results. Figure 3A, C and E show that the TSAT yield increased with increasing ethanol concentrations, ultrasound time and solid–liquid ratio, but further increases in the levels of these factors did not result in greater yields. This result is consistent with the single-factor test. The response surface analysis showed significant interactions between X_1X_2 , X_1X_4 and X_2X_4 ($p < 0.05$). Figure 3 shows the trend of increasing TSAT yield with increasing ultrasound temperature, ethanol concentration and solid–liquid ratio, followed by

a slight decrease. However, the circular 3D surface and contour plots indicate that the X_1X_3 , X_2X_3 and X_3X_4 interactions were not significant ($p > 0.05$). The results are consistent with the ANOVA.

Validation of the Optimized Model

The optimum process conditions for TSAT obtained with BBD-RSM were as follows: an ethanol concentration (X_1) of 72.55%, ultrasound time (X_2) of 34.09 min, ultrasound temperature (X_3) of 61.24°C and solid–liquid ratio (X_4) of 16.29 g/mL. Considering the feasibility of the experimental operation, the optimum conditions were modified as follows: ethanol concentration of 73%, ultrasound time of 34 min, ultrasound temperature of 61°C and solid–liquid ratio of 16 g/mL. Subsequently, validation experiments

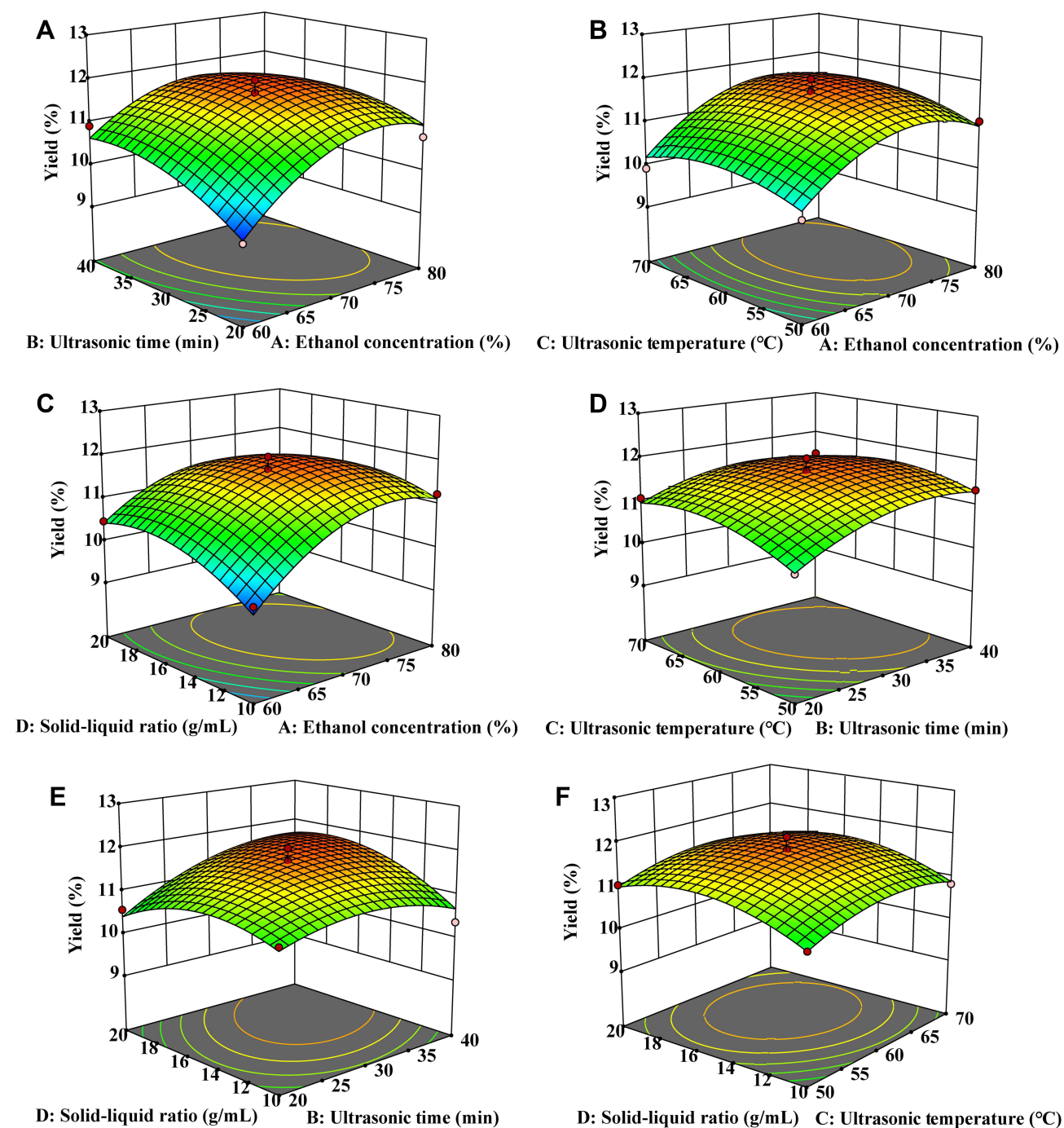


Figure 3 Response surface plots showing the interaction between different variables on the TSAT yield. (A) ultrasonic time and ethanol concentration; (B) ultrasonic temperature and ethanol concentration; (C) solid-liquid ratio and ethanol concentration; (D) ultrasonic temperature and ultrasonic time; (E) solid-liquid ratio and ultrasonic time; (F) solid-liquid ratio and ultrasonic temperature.

were conducted by numerical optimization three times in parallel to confirm the reliability of the predicted model. The TSAT yield from the validation experiments was $11.83 \pm 0.108\%$, which was consistent with the theoretical value (11.88%). These results confirm that the response surface model adequately reflects the desired optimized conditions.

In this study, HRE was also performed to confirm the superiority of UAE of TSAT. The TSAT yield obtained using UAE under optimized conditions was higher than that obtained by HRE ($11.53 \pm 0.124\%$). Admittedly, many previous studies have reported that UAE resulted in a higher content of active ingredients than HRE.^{36,37}

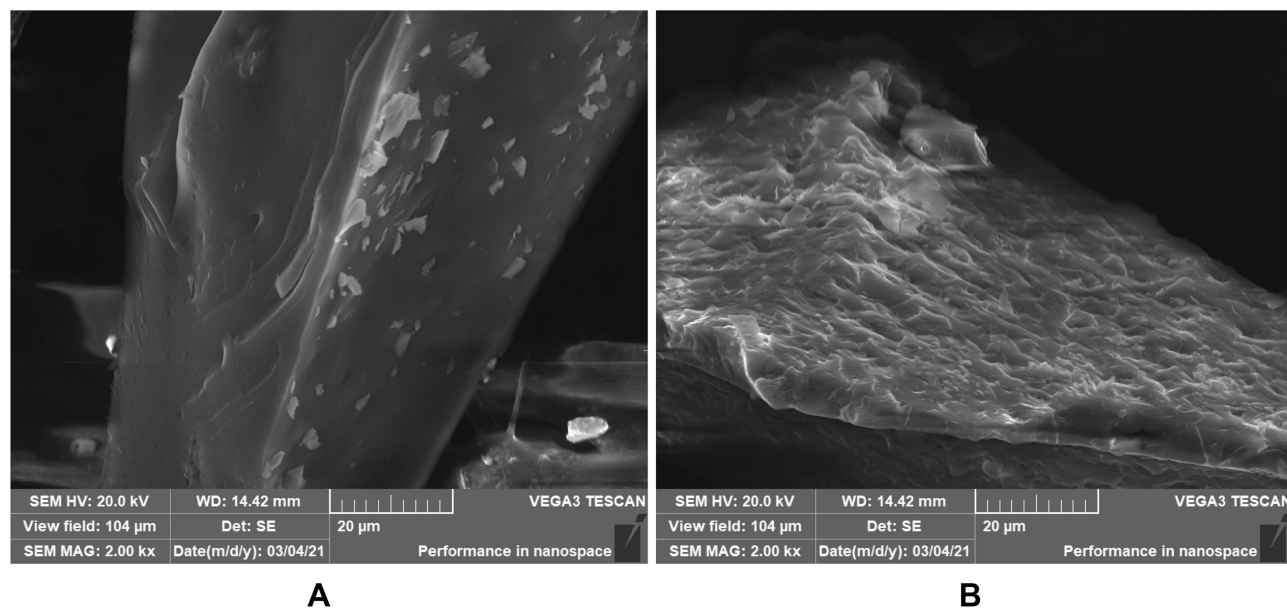


Figure 4 SEM images of the powder before (A) and after ultrasonic treatment (B). Images were taken at 1000× magnification.

SEM Measurements

SEM was used to further reveal the potential mechanism of UAE. Compared to the pre-extraction sample (Figure 4A), the image captured at a magnification of 1000× clearly shows the debris on the surface of TSAT obtained using the UAE method, as well as the enlarged pores (Figure 4B), indicating cell rupture and cell structure damage after UAE, which facilitates easier and more efficient penetration of the solvent into the plant. Similar conclusions were drawn by other researchers who reported that ultrasound-induced “acoustic cavitation” led to changes in the plant fibre structure.³⁸

Validation of the Method for the Quantitative Analysis of Six Saponins

Supplementary Table S1 lists the linear equation, correlation coefficient (R^2), linear range, LOD, and LOQ of each compound determined. All calibration curves showed good linearity ($R^2 \geq 0.9991$) within the tested concentration range. For these compounds, the LOD values ranged from 0.61–9.74 $\mu\text{g/mL}$, while the LOQ values ranged from 1.18–18.51 $\mu\text{g/mL}$. The results of the precision, stability and accuracy tests are shown in Supplementary Table S2. The RSD values for both intraday and interday precision ranged from 1.57–2.09% and 1.75–2.75%, respectively, which indicated the good precision of the developed method. The results of the stability test showed

that the RSD values for the peak areas of all six compounds were $<2.85\%$, indicating that the sample was stable for 12 h at room temperature. According to the calculation, the mean recoveries of the six compounds ranged from 98.14–99.68%, with RSD values ranging from 0.71–1.42%, suggesting the good accuracy of the developed method. In summary, the validation tests showed that the developed method was feasible for the simultaneous quantification of the six compounds in TSAT.

HPLC Analysis of Saponins in the Extracts

Undoubtedly, the pharmacological activity of *A. taibaiensis* depends on its chemical composition. Therefore, the saponins in the *A. taibaiensis* extract were analysed using HPLC. Figure 5 shows highly similar characteristics of the HPLC profiles of the extracts obtained using UAE and HRE. Six triterpenoid saponins were identified, including tarasaponin IV, araloside C, stipuleanoside R2, pseudoginsenoside RT1, araloside A and Chikusetsu saponin IVa, with retention times of 44.661, 45.298, 46.959, 50.598, 51.703 and 53.701 min, respectively. Based on the results of the quantitative HPLC analysis, the contents of the six saponins (mg/g plant material, dry weight) were in the following descending order: araloside A (32.679 ± 0.137 mg/g) > araloside C (23.405 ± 0.159 mg/g) > stipuleanoside R2 (22.216 ± 0.120 mg/g) > tarasaponin IV (13.143 ± 0.114 mg/g) >

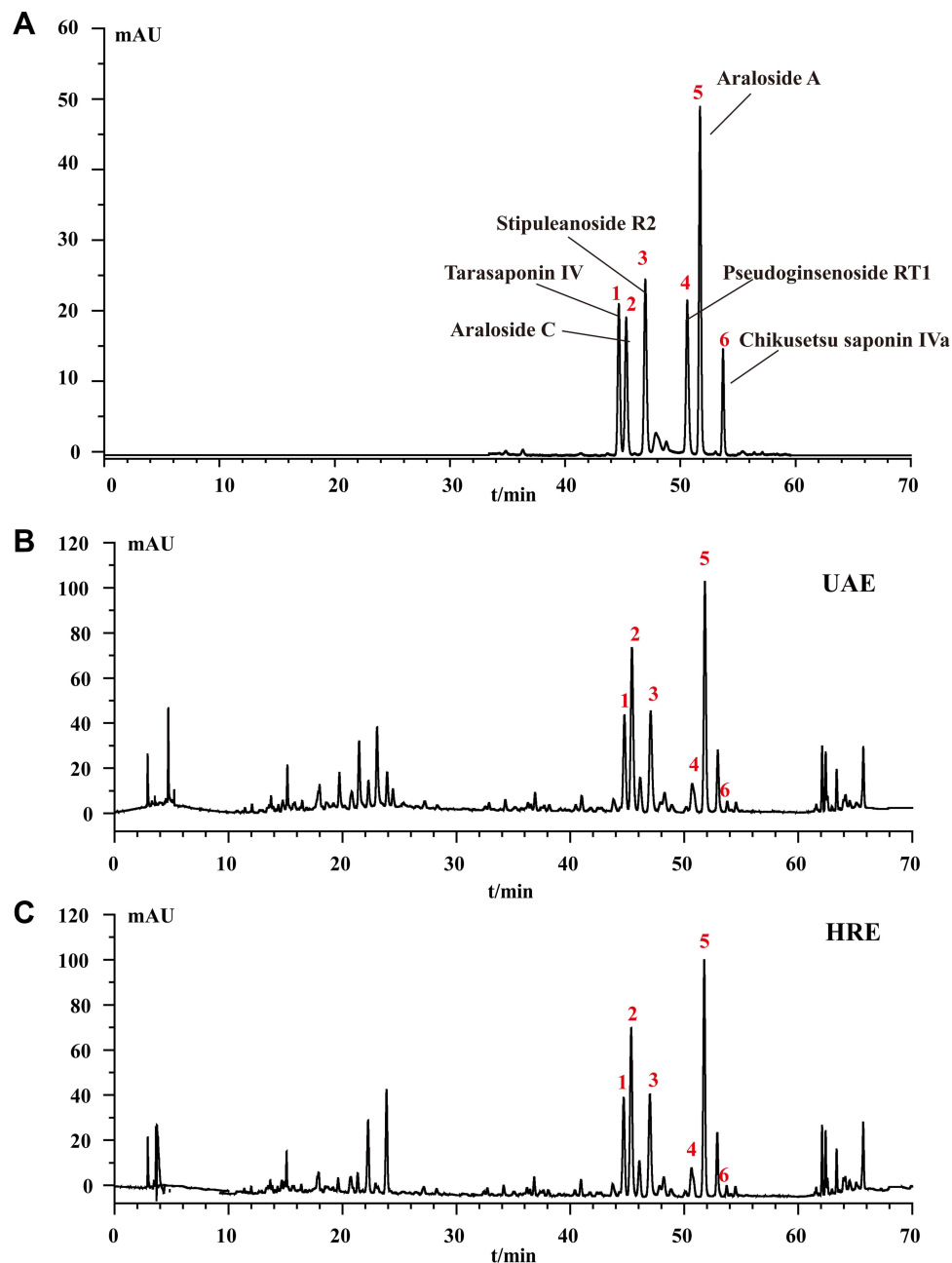


Figure 5 HPLC profiles of standard mixtures (A) and TSAT obtained by optimized UAE (B). TSAT obtained by HRE (C). Peaks: (1) Tarasaponin IV, (2) araloside C, (3) stipuleanoside R2, (4) pseudoginsenoside RT1, (5) araloside A and (6) chikusetsu saponin IVa.

pseudoginsenoside RT1 (8.863 ± 0.114 mg/g) > Chikusetsu saponin IVa (2.203 ± 0.049 mg/g). However, the contents of six saponins extracted using HRE were all lower than those extracted using UAE: araloside A (29.844 ± 0.242 mg/g) > araloside C (21.358 ± 0.179 mg/g) > stipuleanoside R2 (20.281 ± 0.151 mg/g) > tarasaponin IV (12.025 ± 0.099 mg/g) > pseudoginsenoside RT1 (7.978 ± 0.188 mg/g) > Chikusetsu saponin Iva

(1.936 ± 0.041 mg/g). Thus, UAE will be a promising extraction method for the separation of bioactive saponins from *A. taibaiensis* in the future.

α -Glucosidase Inhibition

As shown in Figure 6A, TSAT and its active compounds exerted a dose-dependent effect on inhibiting α -glucosidase. The concentrations of TSAT, tarasaponin IV, araloside C,

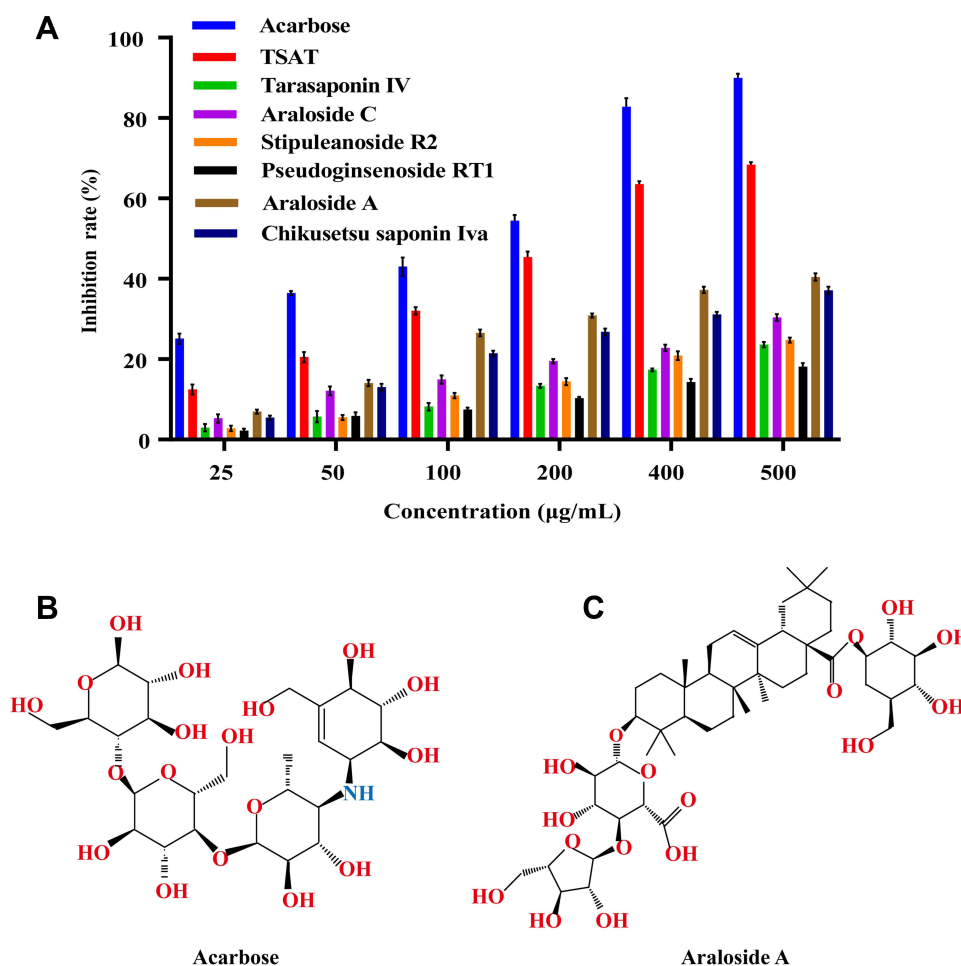


Figure 6 (A) α -Glucosidase inhibitory activity of acarbose, TSAT, tarasaponin IV, araloside C, stipuleanoside R2, pseudoginsenoside RT1, araloside A and chikusetsu saponin IVa. Structures of acarbose (**B**) and araloside A (**C**).

stipuleanoside R2, pseudoginsenoside RT1, araloside A and Chikusetsu saponin IVa resulting in a 50% loss of enzyme activity were determined to be 0.224 mg/mL, 2.939 mg/mL, 2.688 mg/mL, 2.287 mg/mL, 6.011 mg/mL, 0.809 mg/mL and 1.133 mg/mL, respectively. The IC_{50} values for acarbose (**Figure 6B**) measured under the same conditions were much smaller than those for TSAT and its target components, but inhibition of α -glucosidase by TSAT and its six target components was still evident. The IC_{50} values for TSAT towards α -glucosidase were lower than those previously reported (0.48 mg/mL).¹² This discrepancy may be due to slight differences in the composition of the active compounds in TSAT obtained under different conditions. The strong inhibition of α -glucosidase by TSAT compared to the pure compounds might be attributed to the synergistic effect of the multiple active components in the TSAT, as reported in a previous study.¹¹ Previous studies have shown

that sugar substitutions at the C-3 and C-28 positions attached to the pentacyclic triterpene backbone contribute to increased inhibitory activity against α -glucosidase.¹³ Additionally, the inhibitory activity is enhanced by the presence of two neighbouring methyl groups at the C-20 position on the E ring, which are electron-donating groups such as hydroxyl groups attached to the unsaturated C. The interposition of the hydroxyl group is reported to inhibit activity by decreasing the electron cloud density of the I-band on the E ring, while the neighbouring hydroxyl group increases the inhibitory activity.^{1,39} These results explain the α -glucosidase inhibitory activity of *A. taibaiensis* containing mainly pentacyclic triterpenoid saponins. Araloside A (**Figure 6C**) may be the main contributor to the good α -glucosidase inhibitory ability of TSAT; however, the detailed conformational relationship of araloside A requires further study.

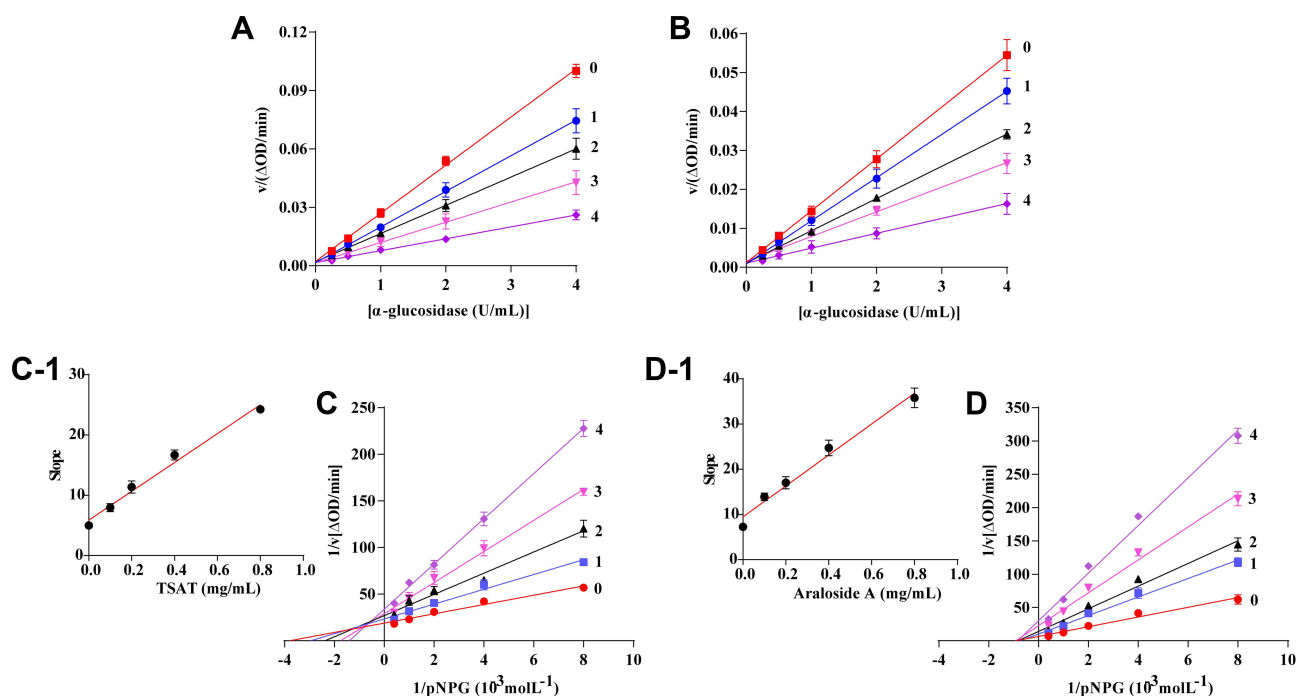


Figure 7 Reversible test and Lineweaver–Burk plots of TSAT/alaroside A against α -glucosidase. **(A)** Reversible test plots of v vs $[\alpha$ -glucosidase]. The concentrations of TSAT for curves 0–4 were 0, 0.1, 0.2, 0.4 and 0.8 mg/mL. **(B)** Reversible test plots of v vs $[\alpha$ -glucosidase]. The concentrations of araloside A for curves 0–4 were 0, 0.1, 0.2, 0.4 and 0.8 mg/mL, respectively. **(C)** Lineweaver–Burk plots of TSAT against α -glucosidase, c (TSAT) = 0, 0.1, 0.2, 0.4 and 0.8 mg/mL, and inhibition constants of TSAT on α -glucosidase. **(D)** Lineweaver–Burk plots of araloside A against α -glucosidase. c (Araloside A) = 0, 0.1, 0.2, 0.4 and 0.8 mg/mL; inhibition constants of araloside A on α -glucosidase.

Kinetics of Inhibition

A plot of V versus $[\alpha$ -glucosidase] in the presence of different concentrations of TSAT or araloside A is shown in Figure 7. If the plot of V against the enzyme concentration passes through the origin, it indicates reversible inhibition. In our study, all straight lines crossed the origin of the coordinates and the slope decreased with increasing drug concentration. Figure 7A and B shows reversible inhibition of α -glucosidase activity by TSAT or araloside A, respectively.

Lineweaver-Burk plots were constructed to understand the inhibitory behaviours and mechanisms of inhibition, and the plots are shown in Figure 7C and D. In the Lineweaver-Burk plots, a series of lines intersected in the second quadrant for the reactions containing different concentrations of TSAT, and the maximum reaction rate V_{max} decreased and the Michaelis constant K_m decreased, suggesting that TSAT exhibits a mixed inhibitory mechanism for α -glucosidase. Mixed inhibition is an intermediate between competitive and noncompetitive inhibition. Namely, TSAT was able to bind free α -glucosidase and α -glucosidase-substrate complexes to inhibit α -glucosidase activity. This finding is consistent with the previously

reported results of inhibition of α -glucosidase by quinoa bran total saponin and rooibos total saponin through mixed competition.^{40,41} In Figure 7D, all the lines also crossed quadrants 1, 2 and 3 but intersected in the negative direction of the x-axis in the Lineweaver-Burk plot, the K_m values remained constant, and the V_{max} decreased with increasing concentrations of araloside A, suggesting that araloside A is a noncompetitive inhibitor. Ding et al¹ also reported that the pentacyclic triterpenoid oleanolic acid was a noncompetitive inhibitor of α -glucosidase. The secondary replot of slope vs [TSAT/alaroside A] was linear (Figure 7C-1, D-1), suggesting that TSAT/alaroside A had a single inhibition site or a single class of inhibition sites on α -glucosidase.

Fluorescence Intensity

Fluorescence spectroscopy was used to further investigate the interaction between TSAT or araloside A and α -glucosidase. The fluorescence emission spectra of α -glucosidase in the presence/absence of TSAT or araloside A were measured at different temperatures ($T=298$ K and 310 K, $\lambda_{exc}=280$ nm). As shown in Figure 8, a strong emission peak near 334 nm was observed in the α -glucosidase spectrum, whereas almost

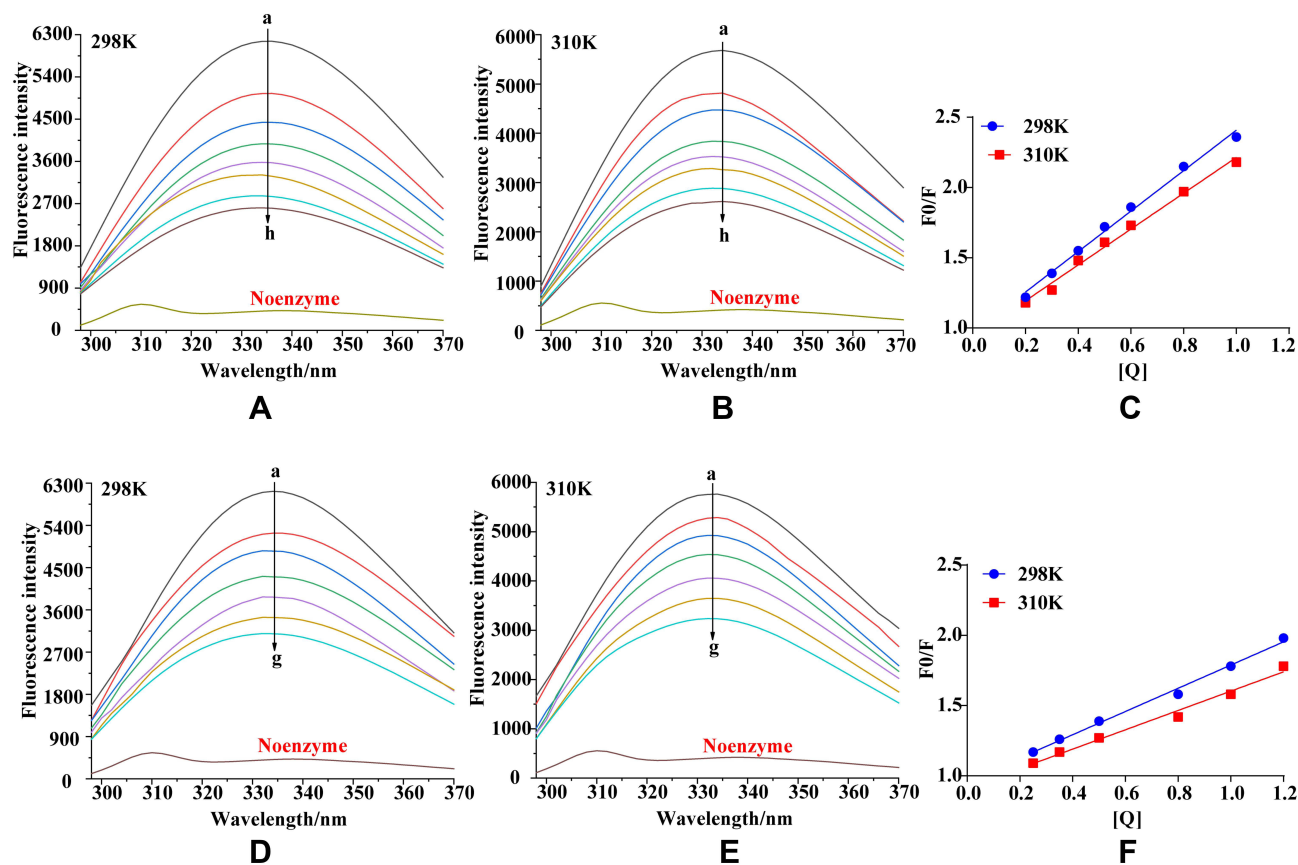


Figure 8 Fluorescence spectra of α -glucosidase in the presence of TSAT at different temperatures (pH 7.0, $\lambda_{\text{ex}} = 280$ nm): **(A)** T=298 K and **(B)** T=310 K. c (α -glucosidase) = 0.1 U/mL, c (TSAT) = 0, 0.2, 0.3, 0.4, 0.5, 0.6, 0.8 and 1 mg/mL for curves a \rightarrow h, respectively. **(D)** T=298 K and **(E)** T=310 K. c (α -glucosidase) = 0.1 U/mL, c (araloside **(A)**) = 0, 0.25, 0.35, 0.5, 0.8, 1 and 1.2 mg/mL for curves a \rightarrow g, respectively. **(C and F)** Stern–Volmer plots of α -glucosidase for fluorescence quenching at different temperatures.

no fluorescence from TSAT or araloside A was detected under the same conditions. The absorption in this region may be attributed to the aromatic amino acids in α -glucosidase, with tryptophan being the main contributor.³ The natural fluorescence of the tryptophan residues in glycosidases and their changing values reflect changes in the protein itself and its surroundings.² α -Glucosidase fluorescence intensity decreased sequentially with the addition of TSAT or araloside A and with increasing temperature, providing direct evidence of the interaction of TSAT or araloside A with α -glucosidase. In addition, the position of the emission peak changed slightly following the addition of TSAT or araloside A, resulting in a redshift of the maximum fluorescence from 334 nm to 336 nm. Based on this result, TSAT- α -glucosidase binding or araloside A- α -glucosidase binding alters the microenvironment around α -glucosidase and causes a spatial shift in the α -glucosidase structure.⁴²

Small molecule-enzyme interactions, molecular rearrangements and excited state reactions all cause endogenous fluorescence quenching of proteins, with dynamic and

static quenching identified as the two quenching mechanisms.⁴³ The fluorescence quenching data were analysed using the Stern-Volmer equation to elucidate the probable quenching mechanism between TSAT, araloside A and α -glucosidase:

$$\frac{F_0}{F} = 1 + K_q \tau_0 [Q] = 1 + K_{sv} [Q] \quad (6)$$

where F_0 and F are the fluorescence intensities (334 nm) of the enzyme in the absence and presence of different concentrations of TSAT/araloside A, respectively. $[Q]$ is the corresponding concentration of TSAT and araloside A. K_{sv} is the Stern-Volmer quenching constant ($K_{sv} = K_q \tau_0$), which is determined from a linear regression analysis of a plot of F_0/F against $[Q]$. K_q is the quenching rate constant, and τ_0 is the average lifetime of the fluorophore without a quencher (the value of τ_0 for the biopolymer is 10^{-8} s).

As shown in **Figure 8**, all Stern-Volmer plots linearly fit the regression equation well ($R^2 > 0.99$). The values of K_{sv} decreased with increasing temperature, indicating the

Table 5 The Quenching Constants (K_{SV}), Binding Constants (K_a), Number of Binding Sites (n) and Relative Thermodynamic Parameters for the Interaction Between TSAT/Araloside A and α -Glucosidase at Different Temperatures

	T(K)	K _{sv} ($\times 10^3$ L/g)	R ^a	K _a ($\times 10^3$ L/g)	n	R ^b	ΔH (KJ/g)	ΔG (KJ/g)	ΔS (J/g/k)
TSAT	298	1.44 \pm 0.05	0.994	1.29 \pm 0.08	1.13 \pm 0.02	0.991	-8.54 \pm 0.2	-40.86 \pm 0.3	108.46 \pm 0.3
	310	1.28 \pm 0.03	0.991	1.13 \pm 0.05	1.20 \pm 0.03	0.984		-41.72 \pm 0.2	
Araloside A	298	0.83 \pm 0.02	0.994	1.18 \pm 0.04	1.07 \pm 0.03	0.991	-11.69 \pm 0.1	-40.34 \pm 0.3	135.33 \pm 0.2
	310	0.69 \pm 0.03	0.987	0.98 \pm 0.03	1.29 \pm 0.02	0.998		-40.88 \pm 0.1	

presence of static quenching. Static quenching is caused by the formation of a nonfluorescent ground state complex between the quencher and the protein fluorescent moiety rather than a dynamic collision. Thus, the formation of the TSAT- α -glucosidase complex or the araloside A- α -glucosidase complex is the primary cause of α -glucosidase fluorescence quenching.³

Binding Constant and Number of Binding Sites

For static quenching, an improved method was used to calculate the binding constant (K_a) and the number of binding sites (n):

$$\log \frac{F_0 - F}{F} = n \log K_a - n \log \frac{1}{[Q_t] - \frac{(F_0 - F)[P_t]}{F_0}} \quad (7)$$

F₀ and F are the same as in Equation (6); [Pt] and [Qt] indicate the total concentrations of α -glucosidase and TSAT/araloside A, respectively. The values of K_a (the binding constant) and n (the number of binding sites per enzyme molecule) were calculated from the slope and intercept of the plots of log(F₀-F)/F versus log([Qt]-[Pt](F₀-F)/F), and the results are summarized in Table 5. The value of n was approximately equal to 1, indicating that TSAT/araloside A has one binding site or class of inhibition sites in α -glucosidase, consistent with the results of the Lineweaver-Burk plot. The K_a values at 298 K were 1.29 $\times 10^3$ L/g and 1.18 $\times 10^3$ L/g, indicating a high affinity between TSAT/araloside A and α -glucosidase. The trend of decreasing K_a with increasing temperature indicated that the stability of the TSAT/araloside A- α -glucosidase complex decreased at higher temperatures.⁴⁴ The results further reveal that fluorescence quenching is a static quenching process.

Thermodynamic Analysis and Binding Forces

Four main types of noncovalent interactions occur between the ligand and macromolecule, ie, electrostatic interactions, multiple hydrogen bonds, van der Waals interactions and hydrophobic forces. The thermodynamic parameters (enthalpy change ΔH , entropy change ΔS and free energy change ΔG) were determined using the van't Hoff equation (Equation 8 and Equation 9) to further determine the type of binding force between TSAT or arachidonic A and α -glucosidase. If little change in temperature is observed, then ΔH can be considered a constant. Therefore, ΔH , ΔS and ΔG values were evaluated using the van't Hoff equation as follows:

$$\log K_a = -\frac{\Delta H}{2.303RT} + \frac{\Delta S}{2.303R} \quad (8)$$

and

$$\Delta G = \Delta H - T\Delta S \quad (9)$$

where K_a is the binding constant at the corresponding temperature (T), T represents the absolute temperature used in the experiment and R is the gas constant (8.314 J mol⁻¹K⁻¹). The plot between log K_a and 1/T showed good linearity, from which the values of ΔH and ΔS were obtained. The negative value of ΔG indicated that the interaction between TSAT/araloside A and α -glucosidase was spontaneous, and the negative value of ΔH indicated that the interaction is an exothermic process, consistent with the decreasing trend of K_a with temperature.⁴⁵ Furthermore, positive values for ΔS and negative values for ΔH suggest that hydrogen bonding and hydrophobic forces are the main forces driving the interaction between TSAT/araloside A and α -glucosidase.²

AFM Studies

AFM has been used to study the structure of biomolecules. In this study, we used the AFM knock pattern to study the

interaction between araloside A and α -glucosidase. As shown in **Figure 9A** and **C** free α -glucosidase was clearly visible and distributed on the surface of mica. However, when araloside A was added, free α -glucosidase appeared to aggregate. As shown in **Figure 9B** and **D**, free proteases such as α -glucosidase, trypsin, and tyrosinase are among the different molecules that participate in hydrophobic interactions and hydrogen bonding. A stable structure is formed under force. Once the balance of intermolecular forces is disrupted, proteases may aggregate to form a new stable body that reduces the water contact.⁴⁶ After araloside A was mixed with α -glucosidase, it changed the microenvironment around the α -glucosidase molecule, exposing the protein structure to a more hydrophobic environment. α -Glucosidase began to accumulate and increase to reduce the surface area in contact with water

and form a stable structure.⁴⁷ Therefore, agglomerated α -glucosidase was observed, indicating that a hydrophobic interaction formed between araloside A and α -glucosidase.

FT-IR

To further determine the structure changes of enzymes by araloside A, the interactions of α -glucosidase with araloside A were analysed by FT-IR spectroscopy.⁴⁸ As shown in **Figure 10**, no new characteristic peaks appeared in the FT-IR spectra of the α -glucosidase-araloside A composites, indicating that no new covalent bonds formed during their interaction.⁴⁹ It has been reported that enzymes containing several amide bands would exert signals in the region 1700–1600 and 1600–1500 cm^{-1} , representing the stretching vibration of C=O (amide I) and N-H (amide II), respectively.^{50,51} Therefore, the alteration of amide bands is often used in

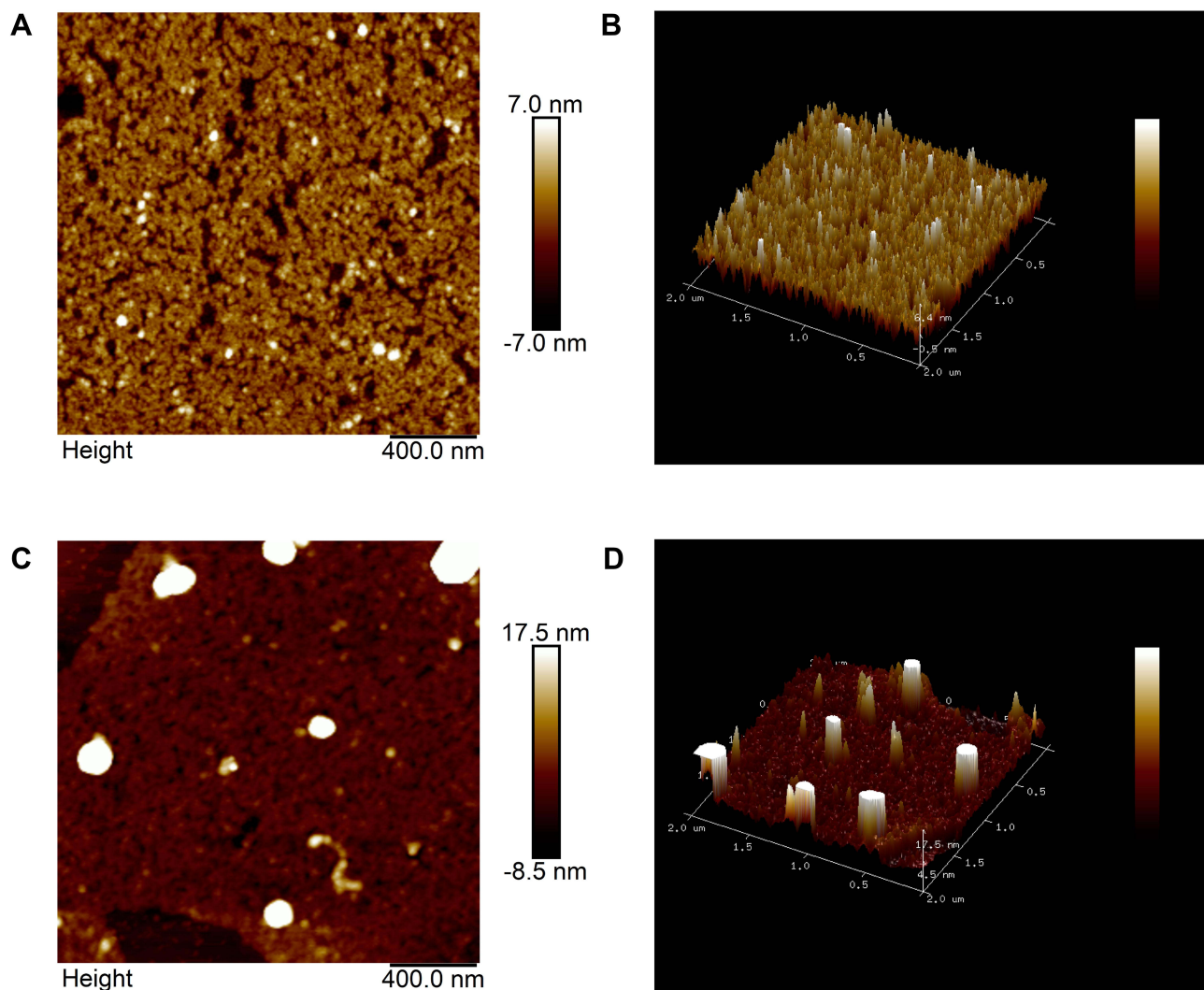


Figure 9 AFM image of free α -glucosidase (**A**) and the araloside A- α -glucosidase complex (**B**). $c(\alpha$ -glucosidase) = 0.1 U/mL, and c (araloside A) = 0.02 mg/mL. (**C** and **D**) are the three-dimensional graphs for panels **A** and **B**, respectively.

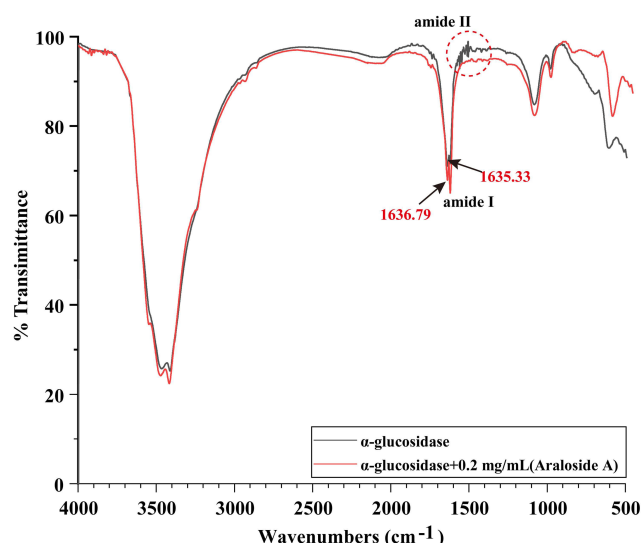


Figure 10 FT-IR spectra of α -glucosidase with araloside A.

characterising the chemical composition and conformation of enzymes. The peak position of amide I (1635.33 cm^{-1}) bands of free α -glucosidase shifted slightly to 1636.79 cm^{-1} and its intensity enhanced with the addition of araloside A, while the amide II bands became smooth or even disappeared with the addition of araloside A. These observations suggested that araloside A interacted with N-H groups, inducing the rearrangement of the polypeptide carbonyl hydrogen bonding pattern and destroying the interaction of amide II groups.⁴⁸

Molecular Simulation of Araloside a Binding to α -Glucosidase

Molecular docking was performed and related structural changes were characterized to further understand the binding mode of araloside A and α -glucosidase. Acarbose was used as a positive control. **Figure 11A** and **B** show the clustering results of the docking conformation of the ligand molecule and the protein. Based on the clustering result in **Figure 11A** with an RMSD of 2.0, the conformation produced by the docking of acarbose is mainly distributed between $-6.0\text{ kcal/mol} \sim -4.0\text{ kcal/mol}$, indicating that the acarbose molecule may form a variety of conformations that match the active pocket of the 3A4A protein, which also shows that the acarbose molecule forms a stable complex with glucosidase. The conformation with the most negative binding energy of acarbose to proteins (-7.63 kcal/mol) was analysed to further evaluate the binding of acarbose molecules to the protein. As shown in **Figure 11D**, the acarbose molecule matched the active pocket of the protein. Multiple residues in the active site form strong hydrogen bonds with the small

molecule acarbose to facilitate an interaction, such as GLU-411, ASP-215, ASP-242, ASP-69 and carboxyl oxygen atoms of other amino acids and acarbose. The protons of the hydroxyl group form stable hydrogen bond interactions. The hydrogen bond distances are 2.4 \AA , 2.4 \AA , 2.9 \AA , and 2.2 \AA , which are much smaller than the traditional hydrogen bond distance of 3.5 \AA . Therefore, acarbose molecules bind tightly to proteins and form a stable complex, preventing them from leaving the pocket. In addition, based on the clustering result graph with an RMSD of 2.0, the conformation produced by the docking of araloside A is mainly distributed between -5.0 kcal/mol and -3.0 kcal/mol , and the docking result is slightly worse than that of acarbose (-5.97 kcal/mol). This difference may be because the two ends of the araloside A molecule are bound to glycosides, the middle exerts a strong hydrophobic effect, and the overall volume is large, which hinders the interaction with the active site of the protein to a certain extent. On the other hand, the hydrophobic chain in the middle will also increase the rigidity of the small molecule, preventing it from twisting to adapt to the active site of the protein. However, combined with the binding mode of araloside A and the active site of the protein (**Figure 11C** and **E**), we found that araloside A partially binds to the surface of the protein and forms multiple hydrogen bond interactions with amino acids such as GLU-411 and ASP-307. The carboxyl oxygen atom and the hydroxyl proton of araloside A form a stable hydrogen bond interaction. The hydrogen bond distances are 1.8 \AA and 2.2 \AA , which are much smaller than the traditional hydrogen bond of 3.5 \AA . Thus, the araloside A molecule also binds tightly to the protein. Small molecules that stabilize the active pocket are very important. In addition, protons on the nitrogen of GLN-279 and ARG-325 form a strong hydrogen bond with the hydroxyl oxygen atom of araloside A. The hydrogen bond distance is short, and the binding affinity is strong, confirming the thermodynamic analysis results. In summary, the araloside A molecule interacts with the active site of α -glucosidase through hydrogen bonding and hydrophobic interactions to form a stable complex, which is consistent with the results of the spectroscopy analysis and provides supporting data for the inhibition of α -glucosidase by araloside A.

Conclusions

In the present study, UAE was proven to be a rapid and efficient method for the extraction of total saponins

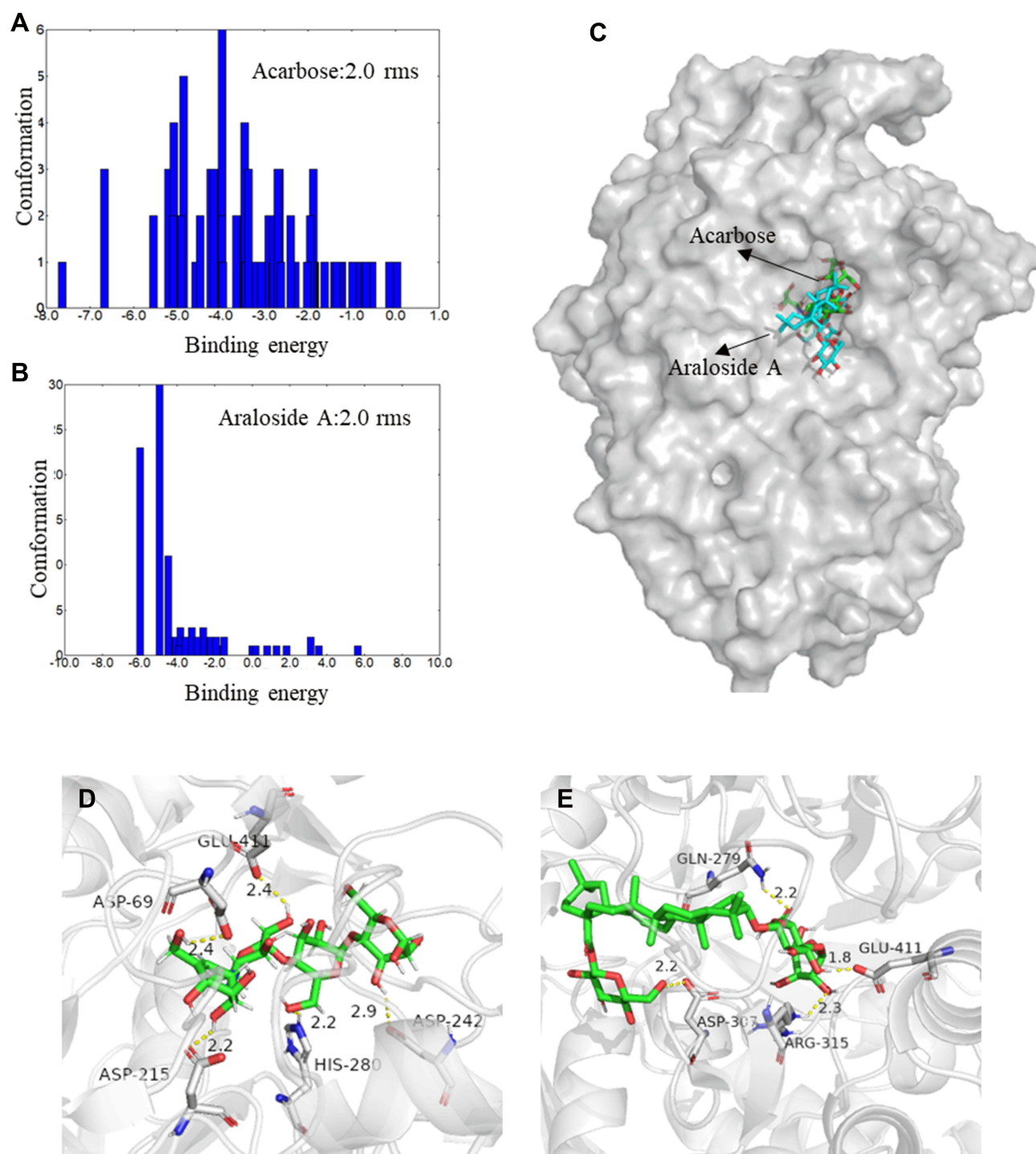


Figure 11 (A and B) Cluster analyses of the AutoDock docking runs of acarbose and araloside A with α -glucosidase. (C) Predicted binding mode of acarbose and araloside A docked with α -glucosidase on the molecular surface. (D) The interaction between acarbose and α -glucosidase. (E) The interaction between araloside A and α -glucosidase. The short solid yellow line stands for hydrogen bonds.

from *A. taibaiensis*, and the optimal process parameters optimized using BBD-RSM were as follows: an ethanol concentration of 73%, ultrasound time of 34 min, ultrasound temperature of 61°C and solid-to-liquid ratio of 16 g/mL. Under optimized UAE conditions, the yield

of TSAT was $11.83 \pm 0.108\%$, which was higher than that obtained using HRE. HPLC analysis further suggested that UAE was more suitable than HRE for the extraction of the six saponins. Furthermore, the TSAT obtained using the optimized UAE method and

araloside A reversibly inhibited α -glucosidase activity in a mixed and noncompetitive manner, respectively. α -Glucosidase fluorescence was quenched by hydrogen bonding and hydrophobic interactions driven by the formation of the TSAT/araloside A- α -glucosidase complex, which was produced spontaneously ($\Delta G < 0$). AFM and FT-IR further showed that the interaction of araloside A with α -glucosidase alters the microenvironment and conformation of the enzyme. Docking results showed that araloside A binds to the cavity of α -glucosidase mainly through hydrogen bonding and hydrophobic interactions to form the araloside A- α -glucosidase complex that leads to a decrease in enzyme activity, supporting the results of thermodynamic analysis. Overall, UAE is a more effective method for extracting total saponins from *Aralia taibaiensis*. In addition, TSAT and its active ingredient, araloside A, exhibit good α -glucosidase inhibition and show potential as a natural ingredient in functional foods to control postprandial blood glucose levels.

Author Contributions

All authors made a significant contribution to the work reported, whether that is in the conception, study design, execution, acquisition of data, analysis and interpretation, or in all these areas; took part in drafting, revising or critically reviewing the article; gave final approval of the version to be published; have agreed on the journal to which the article has been submitted; and agree to be accountable for all aspects of the work.

Funding

This study was supported by the National Natural Science Foundation of China (No. 81703925) and the Disciplinary Innovation Team Construction Project of Shaanxi University of Chinese Medicine (No. 2019-YL11).

Disclosure

The authors have no conflicts of interest for this work to declare.

References

- Ding H, Hu X, Xu X, Zhang G, Gong D. Inhibitory mechanism of two allosteric inhibitors, oleanolic acid and ursolic acid on α -glucosidase. *Int J Biol Macromol*. 2018;107:1844–1855. doi:10.1016/j.ijbiomac.2017.10.040
- Zeng L, Zhang G, Liao Y, Gong D. Inhibitory mechanism of morin on α -glucosidase and its anti-glycation properties. *Food Funct*. 2016;7(9):3953–3963. doi:10.1039/c6fo00680a
- Wang H, Wang J, Liu Y, Ji Y, Guo Y, Zhao J. Interaction mechanism of carnosic acid against glycosidase (α -amylase and α -glucosidase). *Int J Biol Macromol*. 2019;138:846–853. doi:10.1016/j.ijbiomac.2019.07.179
- Alqahtani A, Hamid K, Kam A, et al. The pentacyclic triterpenoids in herbal medicines and their pharmacological activities in diabetes and diabetic complications. *Curr Med Chem*. 2013;20(7):908–931. doi:10.2174/0929867311320070007
- Li Y, Xiang Z, Cui H, et al. Two new oleanane-type saponins from the husks of *Xanthoceras sorbifolia* Bunge. *Nat Prod Res*. 2013;27(3):208–214. doi:10.1080/14786419.2012.666748
- Woo K, Cha J, Choi S, Lee K. A new triterpene glycoside from the stems of *Lagerstroemia indica*. *Arch Pharm Res*. 2016;39(5):631–635. doi:10.1007/s12272-016-0746-4
- Hou W, Li Y, Zhang Q, et al. Triterpene acids isolated from *Lagerstroemia speciosa* leaves as α -glucosidase inhibitors. *Phytother Res*. 2009;23(5):614–618. doi:10.1002/ptr.2661
- Ding H, Wu X, Pan J, Hu X, Gong D, Zhang G. New insights into the inhibition mechanism of betulinic acid on α -Glucosidase. *J Agric Food Chem*. 2018;66(27):7065–7075. doi:10.1021/acs.jafc.8b02992
- Xi M, Hai C, Tang H, et al. Antioxidant and antiglycation properties of triterpenoid saponins from *Aralia taibaiensis* traditionally used for treating diabetes mellitus. *Redox Rep*. 2010;15(1):20–28. doi:10.1179/174329210x12650506623041
- Xi M, Hai C, Tang H, Chen M, Fang K, Liang X. Antioxidant and antiglycation properties of total saponins extracted from traditional Chinese medicine used to treat diabetes mellitus. *Phytother Res*. 2008;22(2):228–237. doi:10.1002/ptr.2297
- Cui J, Li Y, Jia N, et al. Insulin-secretagogue activity of eleven plant extracts and twelve pure compounds isolated from *Aralia taibaiensis*. *Life Sci*. 2013;92(2):131–136. doi:10.1016/j.lfs.2012.11.014
- Dou F, Xi M, Wang J, et al. α -Glucosidase and α -amylase inhibitory activities of saponins from traditional Chinese medicines in the treatment of diabetes mellitus. *Die Pharmazie*. 2013;68(4):300–304.
- Bi L, Tian X, Dou F, Hong L, Tang H, Wang S. New antioxidant and antiglycation active triterpenoid saponins from the root bark of *Aralia taibaiensis*. *Fitoterapia*. 2012;83(1):234–240. doi:10.1016/j.fitote.2011.11.002
- Zhao S, Kwok K, Liang H. Radix Bupleuri Investigation on ultrasound assisted extraction of saikosaponins from. *Sep Purif Technol*. 2007;55(3):307–312. doi:10.1016/j.seppur.2006.12.002
- Hadidi M, Ibarz A, Pagan J. Optimisation and kinetic study of the ultrasonic-assisted extraction of total saponins from alfalfa (*Medicago sativa*) and its bioaccessibility using the response surface methodology. *Food Chem*. 2020;309:125786. doi:10.1016/j.foodchem.2019.125786
- Rostagno M, Palma M, Barroso C. Ultrasound-assisted extraction of soy isoflavones. *J Chromatogr A*. 2003;1012(2):119–128. doi:10.1016/s0021-9673(03)01184-1
- Fu X, Belwal T, Cravotto G, Luo Z. Sono-physical and sono-chemical effects of ultrasound: primary applications in extraction and freezing operations and influence on food components. *Ultrason Sonochem*. 2020;60:104726. doi:10.1016/j.ultsonch.2019.104726
- Chemat F, Rombaut N, Sicaire A, Meullemiestre A, Fabiano-Tixier A, Abert-Vian M. Ultrasound assisted extraction of food and natural products. Mechanisms, techniques, combinations, protocols and applications. A review. *Ultrason Sonochem*. 2017;34:540–560. doi:10.1016/j.ultsonch.2016.06.035
- Wen L, Zhang Z, Sun D, Sivagnanam S, Tiwari B. Combination of emerging technologies for the extraction of bioactive compounds. *Crit Rev Food Sci Nutr*. 2020;60(11):1826–1841. doi:10.1080/10408398.2019.1602823

20. Dranca F, Oroian M. Optimization of ultrasound-assisted extraction of total monomeric anthocyanin (TMA) and total phenolic content (TPC) from eggplant (*Solanum melongena* L.) peel. *Ultrason Sonochem*. 2016;31:637–646. doi:10.1016/j.ultsonch.2015.11.008
21. Ammar A, Naoufal L, Azam B, Dennis W, David L. Phytochemicals: extraction, isolation, and identification of bioactive compounds from plant extracts. *Plants*. 2017;6(4):42. doi:10.3390/plants6040042
22. Deng J, Liu Q, Zhang C, Cao W, Fan D, Yang H. Extraction optimization of polyphenols from waste kiwi fruit seeds (*Actinidia chinensis* Planch.) and evaluation of its antioxidant and anti-inflammatory properties. *Molecules*. 2016;21(7):832. doi:10.3390/molecules21070832
23. Hu T, Guo Y, Zhou Q, et al. Optimization of ultrasonic-assisted extraction of total saponins from *Eclipta prostrata* L. using response surface methodology. *J Food Sci*. 2012;77(9):C975–82. doi:10.1111/j.1750-3841.2012.02869.x
24. Quintero Quiroz J, Naranjo Duran A, Silva Garcia M, Ciro Gomez G, Rojas Camargo J. Ultrasound-assisted extraction of bioactive compounds from annatto seeds, evaluation of their antimicrobial and antioxidant activity, and identification of main compounds by LC/ESI-MS analysis. *Int J Food Sci*. 2019;2019:3721828. doi:10.1155/2019/3721828
25. Yolmeh M, Habibi Najafi M, Farhoosh R. Optimisation of ultrasound-assisted extraction of natural pigment from annatto seeds by response surface methodology (RSM). *Food Chem*. 2014;155:319–324. doi:10.1016/j.foodchem.2014.01.059
26. Li W, Zhao L, Sun Y, et al. Optimization of pressurized liquid extraction of three major acetophenones from *Cynanchum bungei* using a box-behken design. *Int J Mol Sci*. 2012;13(11):14533–14544. doi:10.3390/ijms131114533
27. Li H, Zhai B, Sun J, et al. *Aralia taibaiensis* antioxidant, anti-aging and organ protective effects of total saponins from. *Drug Des Devel Ther*. 2021;15:4025–4042. doi:10.2147/dddt.S330222
28. Bae I, Ham H, Jeong M, Kim D, Kim H. Simultaneous determination of 15 phenolic compounds and caffeine in teas and mate using RP-HPLC/UV detection: method development and optimization of extraction process. *Food Chem*. 2015;172:469–475. doi:10.1016/j.foodchem.2014.09.050
29. Zhou F, Zhang L, Gu L, et al. Simultaneous quantification of 13 compounds in guanxin shutong capsule by HPLC method. *J Chromatogr Sci*. 2016;54(6):971–976. doi:10.1093/chromsci/bmw029
30. Chai W, Wei M, Wang R, Deng R, Zou Z, Peng Y. Avocado proanthocyanidins as a source of tyrosinase inhibitors: structure characterization, inhibitory activity, and mechanism. *J Agric Food Chem*. 2015;63(33):7381–7387. doi:10.1021/acs.jafc.5b03099
31. Yang B, Zhang M, Weng H, Xu Y, Zeng L. Anoechilus Optimization of Ultrasound Assisted Extraction (UAE) of Kinsenoside Compound from (Wall.) Lindl by Response Surface Methodology (RSM). *Molecules*. 2020;25(1). doi:10.3390/molecules25010193
32. Kumar K, Srivastav S, Sharanagat V. Ultrasound assisted extraction (UAE) of bioactive compounds from fruit and vegetable processing by-products: a review. *Ultrason Sonochem*. 2021;70:105325. doi:10.1016/j.ultsonch.2020.105325
33. Shen S, Zhu L, Wu Z, Wang G, Ahmad Z, Chang M. Ganoderma lucidum Production of triterpenoid compounds from spore powder using ultrasound-assisted extraction. *Prep Biochem Biotechnol*. 2020;50(3):302–315. doi:10.1080/10826068.2019.1692218
34. Lee J, Mo E, Choi J, et al. Effect of Korean Red Ginseng extraction conditions on antioxidant activity, extraction yield, and ginsenoside Rg1 and phenolic content: optimization using response surface methodology. *J Ginseng Res*. 2016;40(3):229–236. doi:10.1016/j.jgr.2015.08.001
35. Yang L, Cao Y, Jiang J, Lin Q, Chen J, Zhu L. Response surface optimization of ultrasound-assisted flavonoids extraction from the flower of *Citrus aurantium* L. var. *amara* Engl. *J Sep Sci*. 2010;33(9):1349–1355. doi:10.1002/jssc.200900776
36. Hou M, Hu W, Wang A, et al. Pteris cretica ultrasound-assisted extraction of total flavonoids from L.: process optimization, HPLC analysis, and evaluation of antioxidant activity. *Antioxidants*. 2019;8(10). doi:10.3390/antiox8100425
37. Yang Q, Gan R, Ge Y, Zhang D, Corke A. Phaseolus vulgaris ultrasonic treatment increases extraction rate of common bean (L.) antioxidants. *Antioxidants*. 2019;8(4). doi:10.3390/antiox8040083
38. Shi W, Jia J, Gao Y, Zhao Y. Influence of ultrasonic pretreatment on the yield of bio-oil prepared by thermo-chemical conversion of rice husk in hot-compressed water. *Bioresour Technol*. 2013;146:355–362. doi:10.1016/j.biortech.2013.07.094
39. Wang Y, Zhang G, Pan J, Gong D. Novel insights into the inhibitory mechanism of kaempferol on xanthine oxidase. *J Agric Food Chem*. 2015;63(2):526–534. doi:10.1021/jf505584m
40. Dong Q, Tan L, Hu N, Wang H. Study on the optimization of the extraction technology by response surface methodology and inhibitory activity of α -glucoside of total saponins from the bran of *Chenopodium quinoa* wild. *Nat Prod Res Dev*. 2021;33(6):935–942.
41. Yang W, Li C, Yu K, Liu H, Qi X. Inhibitory effect of mogrosides crude extract on α -glucosidase in vitro. *Sci Technol Food Ind*. 2016;37(24):111–115.
42. Wang M, Shi J, Wang L, et al. Inhibitory kinetics and mechanism of flavonoids from lotus (*Nelumbo nucifera* Gaertn.) leaf against pancreatic α -amylase. *Int J Biol Macromol*. 2018;120:2589–2596. doi:10.1016/j.ijbiomac.2018.09.035
43. Zhang G, Wang L, Pan J. Probing the binding of the flavonoid diosmetin to human serum albumin by multispectroscopic techniques. *J Agric Food Chem*. 2012;60(10):2721–2729. doi:10.1021/jf205260g
44. Zhao D, Zhou A, Du Z, Zhang Y, Zhang K, Ma Y. Coumarins with α -glucosidase and α -amylase inhibitory activities from the flower of *Edgeworthia gardneri*. *Fitoterapia*. 2015;107:122–127. doi:10.1016/j.fitote.2015.10.012
45. Lin M, Chai W, Zheng Y, Huang Q, Ou-Yang C. Inhibitory kinetics and mechanism of rifampicin on α -glucosidase: insights from spectroscopic and molecular docking analyses. *Int J Biol Macromol*. 2019;122:1244–1252. doi:10.1016/j.ijbiomac.2018.09.077
46. Wang Y, Zhang G, Wang L. Potential toxicity of phthalic acid esters plasticizer: interaction of dimethyl phthalate with trypsin in vitro. *J Agric Food Chem*. 2015;63(1):75–84. doi:10.1021/jf5046359
47. Wang C, Wang J, Deng L. Evaluating interaction forces between BSA and rabbit anti-BSA in sulphathiazole sodium, tylosin and levofloxacin solution by AFM. *Nanoscale Res Lett*. 2011;6(1):579. doi:10.1186/1556-276x-6-579
48. Yan J, Zhang G, Pan J, Wang Y. α -Glucosidase inhibition by luteolin: kinetics, interaction and molecular docking. *Int J Biol Macromol*. 2014;64:213–223. doi:10.1016/j.ijbiomac.2013.12.007
49. Yz A, Wy A, Ws A, et al. Inhibition of porcine pancreatic α -amylase activity by chlorogenic acid - ScienceDirect. *J Funct Foods*. 2020;64:103587.
50. Zheng Y, Tian J, Yang W, et al. Inhibition mechanism of ferulic acid against α -amylase and α -glucosidase. *Food Chem*. 2020;317:126346. doi:10.1016/j.foodchem.2020.126346
51. Zhang S, Qiu B, Zhu J, Khan M, Liu X. Investigation of the interaction of 2,4-dimethoxy-6,7-dihydroxyphenanthrene with α -glucosidase using inhibition kinetics, CD, FT-IR and molecular docking methods. *Spectrochim Acta A Mol Biomol Spectrosc*. 2018;203:13–18. doi:10.1016/j.saa.2018.05.077

Drug Design, Development and Therapy

Dovepress

Publish your work in this journal

Drug Design, Development and Therapy is an international, peer-reviewed open-access journal that spans the spectrum of drug design and development through to clinical applications. Clinical outcomes, patient safety, and programs for the development and effective, safe, and sustained use of medicines are a feature of the journal, which has also

been accepted for indexing on PubMed Central. The manuscript management system is completely online and includes a very quick and fair peer-review system, which is all easy to use. Visit <http://www.dovepress.com/testimonials.php> to read real quotes from published authors.

Submit your manuscript here: <https://www.dovepress.com/drug-design-development-and-therapy-journal>